

# Fundamental parameters of B Supergiants from the BCD System

## I. Calibration of the $(\lambda_1, D)$ parameters into $T_{\text{eff}}$ ★ ★ ★ ★ ★

J. Zorec<sup>1</sup>, L. Cidale<sup>2,3,†</sup>, M. L. Arias<sup>2,3</sup>, Y. Frémat<sup>4</sup>, M. F. Muratore<sup>2</sup>, A. F. Torres<sup>2,3</sup>, and C. Martayan<sup>4,5</sup>

<sup>1</sup> Institut d'Astrophysique de Paris, UMR 7095 du CNRS, Université Pierre & Marie Curie, 98bis bd. Arago, 75014 Paris, France

<sup>2</sup> Facultad de Ciencias Astronómicas y Geofísicas, Universidad Nacional de La Plata, Paseo del Bosque S/N, La Plata, Buenos Aires, Argentina

<sup>3</sup> Instituto de Astrofísica de La Plata, (CCT La Plata - CONICET, UNLP), Paseo del Bosque S/N, La Plata, Buenos Aires, Argentina

<sup>4</sup> Royal Observatory of Belgium, 3 av. Circulaire, 1180 Brussels, Belgium

<sup>5</sup> Observatoire de Paris-Meudon, GEPI, UMR8111 du CNRS, 92195 Meudon Cedex, France

Received ..., ; Accepted ...

### ABSTRACT

**Context.** Effective temperatures of early-type supergiants are important to test stellar atmosphere- and internal structure-models of massive and intermediate mass objects at different evolutionary phases. However, these  $T_{\text{eff}}$  values are more or less discrepant depending on the method used to determine them.

**Aims.** We aim to obtain a new calibration of the  $T_{\text{eff}}$  parameter for early-type supergiants as a function of observational quantities that are: a) highly sensitive to the ionization balance in the photosphere and its gas pressure; b) independent of the interstellar extinction; c) as much as possible model-independent.

**Methods.** The observational quantities that best address our aims are the  $(\lambda_1, D)$  parameters of the BCD spectrophotometric system. They describe the energy distribution around the Balmer discontinuity, which is highly sensitive to  $T_{\text{eff}}$  and  $\log g$ . We perform a calibration of the  $(\lambda_1, D)$  parameters into  $T_{\text{eff}}$  using effective temperatures derived with the bolometric-flux method for 217 program stars, whose individual uncertainties are on average  $|\Delta T_{\text{eff}}|/T_{\text{eff}}^f = 0.05$ .

**Results.** We obtain a new and homogeneous calibration of the BCD  $(\lambda_1, D)$  parameters for OB supergiants and revisit the current calibration of the  $(\lambda_1, D)$  zone occupied by dwarfs and giants. The final comparison of calculated with obtained  $T_{\text{eff}}$  values in the  $(\lambda_1, D)$  calibration show that the latter have total uncertainties, which on average are  $\epsilon_{T_{\text{eff}}}/T_{\text{eff}}^f \simeq \pm 0.05$  for all spectral types and luminosity classes.

**Conclusions.** The effective temperatures of OB supergiants derived in this work agree on average within some 2 000 K with other determinations found in the literature, except those issued from wind-free non-LTE plane-parallel models of stellar atmospheres, which produce effective temperatures that can be overestimated by up to more than 5 000 K near  $T_{\text{eff}} = 25\,000$  K.

Since the stellar spectra needed to obtain the  $(\lambda_1, D)$  parameters are of low resolution, a calibration based on the BCD system is useful to study stars and stellar systems like open clusters, associations or stars in galaxies observed with multi-object spectrographs and/or spectro-imaging devices.

**Key words.** Stars: early-type; Stars: fundamental parameters; Stars: spectrophotometry

## 1. Introduction

The effective temperatures of early-type stars of luminosity classes V to III are similar whatever the method used to determine them. Among the most commonly used methods are those based on: fits of the observed absolute spectral

energy distributions (hereafter ASEDs) with Kurucz (1979) line-blanketed stellar atmosphere models; line profile fittings; Strömberg and Geneva photometric color indices. Using Breger's spectrophotometric catalogue (Breger 1976a) for the ASED in the visual range, Morossi & Malagnini (1985) and Malagnini & Morossi (1990) obtained  $T_{\text{eff}}$  values with internal uncertainties below 5%. The uncertainties are of the order of 10%, either when the TD1 far-UV fluxes and IUE low resolution spectra are used in combination with fluxes from Breger's catalogue (Malagnini et al. 1983, 1986; Gulati et al. 1989), or when H and He absorption line profiles are fitted with models (Morossi & Crivellari 1980). In general,  $T_{\text{eff}}$  values derived using calibrated Strömberg and Geneva

Send offprint requests to: J. Zorec: e-mail: zorec@iap.fr

\* Data obtained at OHP, France

\*\* Data obtained at ESO La Silla, Chili

\*\*\* Data obtained in CASLEO operated under agreement between the CONICET and the Universities of La Plata, Córdoba and San Juan, Argentina

† Member of the Carrera del Investigador Científico, CONICET, Argentina

photometric indices present low uncertainties (Balona 1984; Moon & Dworetzky 1985; Castelli 1991; Achmad et al. 1993). However Napiwotzki et al. (1993), based on a critical comparison of several calibrations of Strömrgren intermediate-band  $uvby-\beta$  photometric indices, recommended the use of the calibration done by Moon & Dworetzky (1985), corrected for gravity deviations.

As regards B supergiants, Code et al. (1976) and Underhill et al. (1979) derived effective temperatures based on spectrophotometric observations in the far-UV, visible and near-IR spectral regions. Later, effective temperature determinations for these stars were made using the silicon lines in the optical spectral region, either by fitting the line profiles or by measuring their equivalent widths (Becker & Butler 1990; McErlean et al. 1999; Trundle et al. 2004). Nowadays, methods based on adjustments of He I and He II line profiles, and/or the line intensity ratio Si IV/Si III are preferred (Herrero et al. 2002; Repolust et al. 2004; Martins et al. 2005; Crowther et al. 2006; Benaglia et al. 2007; Markova & Puls 2008; Searle et al. 2008). Recent estimates of the effective temperature of early B-type supergiants have shown that the values obtained with non-LTE blanketed models including winds (hereafter non-LTE BW models) are systematically lower than those derived with models without winds (hereafter wind-free models) (Lefever et al. 2007; Crowther et al. 2006). Differences range roughly from 0 to 6 000 K and they tend to be lower the later the B-sub-spectral type (Markova & Puls 2008). On the other hand, Morossi & Crivellari (1980) noted that the effective temperatures of B-supergiants derived with photometric methods are in general higher than those obtained spectroscopically. Physical characteristics and phenomena like activity and/or instabilities taking place in the extended atmospheric layers affect more significantly the spectral lines than the continuum spectrum. Thus, the genuine signature due to the  $T_{\text{eff}}$  carried by the lines could be somewhat blurred.

The calibrations of effective temperatures for B supergiants are of great importance since these stars are in a significant phase of the evolutionary sequence of massive stars. They are also the main contributors to the chemical and dynamical evolution of galaxies. Accurate effective temperatures are then needed to construct HR diagrams and to test the theories of stellar structure and evolution, as well as to estimate the chemical content of the stellar environment. Effective temperatures are also necessary to study the physical processes in the atmosphere, such as non-radial pulsations or stellar winds (radiative forces; changes in ionization). Regarding the stellar winds, the effective temperatures are particularly useful in discussing terminal velocities, mass loss rates, the bi-stability jump, and the wind momentum luminosity relationship (Kudritzki et al. 2003; Crowther et al. 2006; Markova & Puls 2008).

As a consequence of the large discrepancies found in the  $T_{\text{eff}}$  estimates of B supergiants, the current temperature scale is being revisited (Markova & Puls 2008; Searle et al. 2008). In this context, we present an independent and homogeneous temperature calibration for B-type dwarfs to supergiants, based on the use of the BCD spectrophotometric system (Barbier & Chalonge 1941; Chalonge & Divan 1952). This method has numerous advantages (see §2), mainly because it is

based on : a) measurable quantities that are strongly sensitive to the ionization balance in the stellar atmosphere and to its gas pressure, thus being excellent indicators of  $T_{\text{eff}}$  and  $\log g$ ; b) parameters that describe the visible continuum spectrum, whose atmospheric formation layers are on average deeper than those for spectral lines.

Our first step will be to determine the effective temperatures of our sample of Galactic B-type supergiants. However, to perform a consistent calibration of the BCD ( $\lambda_1, D$ ) parameters for supergiants, we re-determine the calibration into effective temperature of the BCD ( $\lambda_1, D$ ) domain corresponding to B-type dwarfs and giants ( $D$  = size of the Balmer jump;  $\lambda_1$  = mean spectral position of the Balmer discontinuity (BD); see further explanations on these parameters in §2 and Appendix §A). We use a large and homogeneous sample of B stars observed in the BCD system, and newly-derived effective temperatures for all of them, based on the bolometric-flux method (hereafter BFM). We leave for another contribution the discussion of BCD calibrations related to  $\log g$ , visual and bolometric absolute magnitudes.

The present paper is organized as follows: In §2 we briefly describe the BCD spectrophotometric system and the advantages of its use. In §3 we present the BFM on which the determinations of the stellar effective temperature and angular diameter ( $\theta$ ) are based. Observations and the  $T_{\text{eff}}$  values determined with the BFM are presented in §4. The uncertainties of the effective temperatures and angular diameters obtained with the BFM are discussed in §5. Comparisons of our  $T_{\text{eff}}$  and  $\theta$  determinations with those obtained by other authors are given in §6. In §7, we present the empirical temperature calibration curves and discuss the accuracy of the  $T_{\text{eff}}(\lambda_1, D)$  values obtained. A discussion and global conclusions are presented in §8 and §9, respectively.

## 2. The BCD system

The Paris spectrophotometric classification system of stellar spectra, best known as BCD (Barbier-Chalonge-Divan), was defined by Barbier & Chalonge (1941) and Chalonge & Divan (1952). The original presentation of this system is given in French; explanations in English can be found in Dufay (1964); Underhill (1966); Underhill & Doazan (1982); Divan (1992). A short overview of the system is given in Appendix §A. The BCD system is based on four measurable quantities in the continuum spectrum around the BD:  $D$ , the Balmer jump given in dex and determined at  $\lambda 3700 \text{ \AA}$ ;  $\lambda_1$ , the mean spectral position of the BD, usually given as the difference  $\lambda_1 - 3700 \text{ \AA}$ ;  $\Phi_{uv}$ , the gradient of the Balmer energy distribution in the near-UV from  $\lambda 3100$  to  $\lambda 3700 \text{ \AA}$ , given in  $\mu\text{m}$ ;  $\Phi_{rb}$ , the gradient of the Paschen energy distribution in the wavelength interval  $\lambda \lambda 4000-6200 \text{ \AA}$  given in  $\mu\text{m}$ . The sole BCD parameters that are relevant to the present work are:  $D$ , which is a strong function of  $T_{\text{eff}}$ , and  $\lambda_1$  that is very sensitive to  $\log g$ .

The use of the ( $\lambda_1, D$ ) pair to determine the spectral classification and the stellar fundamental parameters presents numerous advantages, not only because the BD is a well visible spectral characteristic for stars ranging from early O to late F spectral types but also because:

a) The parameters  $(\lambda_1, D)$  are obtained from direct measurement on the stellar continuum energy distribution. This implies that, on average, they are relevant to the physical properties of photospheric layers which are deeper than those described by spectral lines;

b) Each MK (Morgan & Keenan) spectral type-luminosity class (SpT/LC) is represented by wide intervals of  $\lambda_1$  and  $D$  values, which implies high SpT/LC classification resolution:  $\lambda_1$  ranges from about 75 Å for dwarfs to -5 Å for supergiants, while  $D$  ranges from near 0.0 dex, for the hottest O stars and F9 stars, to about 0.5 dex, for the A3-4 stars;

c) Typical  $1\sigma$  measurement uncertainties affecting  $D$  and  $\lambda_1$  are:  $\delta D \leq 0.02$  dex and  $\delta \lambda_1 \leq 2$  Å, respectively. Thus, from b) and c) we find that hardly any other classification system has reached such a high resolution, especially concerning the luminosity class;

d) The parameter  $\lambda_1$  is independent of the interstellar medium (ISM) extinction, while  $D$  has a low E(B-V) color excess dependence, roughly  $\delta D = 0.03$  E(B-V) dex, which is almost insensitive to the selective absorption ratio  $R_V = A_V/E(B-V)$ . The  $\delta D$  difference is produced by extrapolation of the Paschen energy distribution from  $\lambda 4000$  Å to  $\lambda 3700$  Å, which carries the ISM reddening of the Paschen continuum. The low ISM extinction dependence is however of great interest for the study of early-type stars, since they are frequently distant and strongly reddened;

e) Spectra needed to obtain the  $(\lambda_1, D)$  measurements are of low resolution (8 Å at the BD). This means that numerous faint stars can be observed with short exposure times. Furthermore, the flux calibrations required to derive the BCD parameters rely on spectral reduction techniques which are easy-to-use and of common practice;

f) The BCD system is generally used for ‘normal’ stars, i.e. objects whose atmospheres can be modeled in the framework of hydrostatic and radiative equilibrium approximations. However, since both the photospheric and the circumstellar components of the BD are spectroscopically well separated, it can also be used to study some ‘peculiar’ objects, like: i) Be stars (Divan & Zorec 1982; Zorec 1986; Zorec & Briot 1991; Chauville et al. 2001; Zorec et al. 2005; Vinicius et al. 2006); ii) objects with the B[e] phenomenon (Cidale et al. 2001); iii) chemically peculiar stars (He-W group) (Cidale et al. 2007).

### 3. The bolometric-flux method (BFM)

To obtain the calibration of the BCD  $(\lambda_1, D)$  parameters into effective temperature, we could simply adopt for each star the average of all the  $T_{\text{eff}}$  values found in the literature. Nevertheless, these quantities were obtained with several heterogeneous methods which carry more or less systematic differences on the estimates of  $T_{\text{eff}}$ . Since most  $T_{\text{eff}}$  determinations are based on adjustment of the observed ASEDs with theoretical ASEDs, or on fittings of line profiles with models, the properties of the studied stars are implicitly assumed to be in accordance with the physical characteristics of the best fitted stellar model atmosphere. Instead, in the present contribution, we preferred to determine the effective temperature by using the total amount of radiated energy, so that the details of its distribution are of

marginal importance and the dependence on models of stellar atmospheres are kept to a minimum. While models of stellar atmospheres produce Balmer jumps which are close to the observed ones, the theoretical  $\lambda_1$  parameter may differ somewhat. In fact,  $\lambda_1$  depends on the distribution of the emergent radiation fluxes near the limit of the Balmer line series, where the theoretical uncertainties concern the treatment of the non-ideal effects in the hydrogen upper level populations (Rohrman et al. 2003).

We decided to adopt a single method for all program stars and to estimate their effective temperatures using its definition, where the incidence of the model-dependence is in principle strongly minimized.

By definition, the effective temperature of a star is:

$$T_{\text{eff}} = \left[ \frac{4f}{\sigma_R \theta^2} \right]^{1/4}, \quad (1)$$

where  $\sigma_R$  is the Štefan-Boltzmann constant;  $f$  is the stellar bolometric radiation flux received at the Earth, corrected for the ISM extinction;  $\theta$  is the angular diameter of the star. If the radiation field coming from the stellar interior were the sole energy source in the atmosphere, the effective temperature deduced from the bolometric flux would be the same as that derived from the analysis of stellar spectra with model atmospheres in radiative and hydrostatic equilibrium. If the bolometric flux  $f$  and the angular diameter  $\theta$  were issued entirely from observations, the  $T_{\text{eff}}$  deduced from Eq. (1) could then also be considered a genuine observational parameter. The BFM was applied in this way by Code et al. (1976) using stellar fluxes observed with the OAO-2 satellite and the angular diameters determined interferometrically (Hanbury Brown et al. 1974). Unfortunately, this could not happen in our case, as we do not have observed fluxes over the entire spectrum, nor do we have angular diameters measured for all program stars. In what follows the effective temperature and the angular diameter derived with the ‘bolometric flux method’ are called  $T_{\text{eff}}^f$  and  $\theta^f$ , respectively.

Blackwell & Shallis (1977) showed that a stellar angular diameter can be well reproduced with observed fluxes in near-IR and model atmospheres. The monochromatic stellar angular diameter is thus given by:

$$\theta_\lambda = 2 \left[ \frac{f_\lambda^o}{\mathcal{F}_\lambda} \right]^{1/2}, \quad (2)$$

where  $f_\lambda^o$  is the absolute monochromatic flux received at the Earth corrected for the ISM extinction,  $\mathcal{F}_\lambda = \pi F_\lambda$  is the emitted monochromatic flux at the stellar surface,  $F_\lambda$  is the so called ‘astrophysical’ flux predicted by a model atmosphere. To represent  $F_\lambda$  we have used the grids of ATLAS9 model atmospheres calculated by Castelli & Kurucz (2003). In wavelengths lying in the Rayleigh-Jeans tail of the energy distribution, not only are the theoretical fluxes nearly independent of model characteristics, but the observed ASEDs also are mildly affected by the ISM extinction. However, they have the inconvenience of being frequently marred by infrared flux excesses of non stellar origin. We decided to calculate Eq. (2) in the red extreme of the Paschen continuum:  $\lambda \lambda 0.58-0.8 \mu\text{m}$ . In this spectral region,

the theoretical radiative fluxes are still only slightly dependent on the particular model characteristics and the layers where this radiation field is formed have local electron temperatures close to  $T_{\text{eff}}$ , so that the color temperature of the energy distribution of OB stars in this wavelength interval also approaches  $T_{\text{eff}}$  closely. While  $T_{\text{eff}}$  derived with Eq. (1) is insensitive to  $\log g$  within the characteristic uncertainties of its determination, the parameter  $\theta_\lambda$  does depend slightly on models. Therefore, in Eq.(2) model atmospheres giving  $F_\lambda$  are chosen for gravity parameters  $\log g = \log g(\beta, T_{\text{eff}})$ , where  $\beta$  is the  $H\beta$ -line index of the uvby- $\beta$  Strömberg photometry. The  $\beta$  parameters used are from the Hauck & Mermillod (1975) compilation and the  $\log g(\beta, T_{\text{eff}})$  relations used are from Castelli & Kurucz (2006). An extensive use of the BFM was made by Underhill et al. (1979), where unfortunately Eqs. (1) and (2) were iterated only twice, which left the derived effective temperatures strongly correlated with their initial approximate values.

### 3.1. Effective temperatures of B-type dwarfs to giants

The ASEDs of our program stars, taken from the literature to calculate  $f$ , are in most cases observed in the wavelength interval ranging from  $\lambda_a \sim 1200\text{-}1300 \text{ \AA}$  to some  $\lambda_b$  in the far-IR. Many times they present intermediate gaps, according to the observational method or the instruments used. On the other hand, the angular diameter has been measured only for a few bright stars. Nevertheless, as in Eq. (1)  $T_{\text{eff}}$  depends on  $f^{1/4}$ , the effective temperature can still be reliably determined even though the unobserved spectral regions are represented using ‘modestly realistic’ model atmospheres, as discussed in §5. The calculation of the effective temperature for dwarfs to giants is based on the following iteration:

- 1) Adopt initial values of  $T_{\text{eff}}^f$  and  $\log g$ ;
- 2) Interpolate the model fluxes in the far-UV and IR spectral regions for the adopted  $(T_{\text{eff}}, \log g)$  values ;
- 3) Calculate the angular diameter  $\theta^f$  using relation (2) in the near IR spectral region as detailed in the explanation following relation (2), and assume  $\theta^f$  independent of the wavelength;
- 4) Calculate the bolometric flux  $f$  as follows:

$$\begin{aligned}
 f &= f_{\text{obs}} \times [1 + \delta] \\
 f_{\text{obs}} &= \int_{\lambda_a}^{\lambda_b} f_\lambda^o d\lambda \\
 \delta &= \delta_{\text{UV}} + \delta_{\text{IR}} \\
 &= \left\{ \frac{\pi}{4} \theta^2 \frac{\int_{\lambda_a}^{\lambda_b} F_\lambda d\lambda}{f_{\text{obs}}} \right\}_{\text{UV}} + \left\{ \frac{\pi}{4} \theta^2 \frac{\int_{\lambda_b}^{\infty} F_\lambda d\lambda}{f_{\text{obs}}} \right\}_{\text{IR}},
 \end{aligned} \tag{3}$$

where  $f_{\text{obs}}$  and  $\delta$  represent, respectively, the contribution of the observed and unobserved spectral regions (extreme-UV, far-UV and IR) to the bolometric flux;  $\lambda_a$  and  $\lambda_b$  delimit the spectral range of ASEDs actually observed;  $f_\lambda^o$  and  $F_\lambda$  have the same meaning as given in Eqs. (1) and (2);

- 5) Introduce the bolometric flux given by (3) into relation (1) to obtain a new estimate of  $T_{\text{eff}}^f$  and accordingly, of  $\log g = \log g(T_{\text{eff}}^f, \beta)$ ;

- 6) Use the new estimates of  $(T_{\text{eff}}^f, \log g)$  to continue the iteration in step 2).

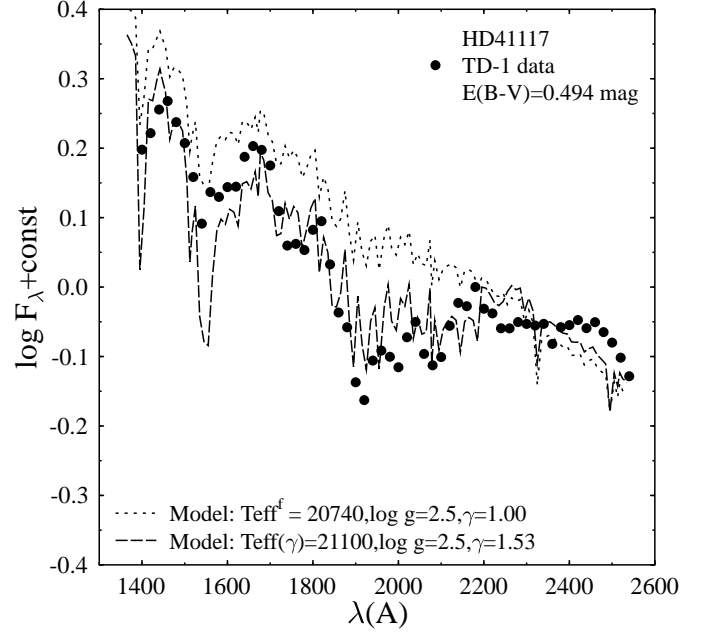


**Fig. 1.** Fitting of the far-UV observed energy distribution of HD 41117 with  $\gamma$ -unmodified model fluxes for  $T_{\text{eff}}^f$  (pointed line), and with  $\gamma$ -modified model for  $T_{\text{eff}}(\gamma)$  (dashed line).

The iterations were performed until the difference between two consecutive  $T_{\text{eff}}^f$  values was smaller than 1 K. Depending on the star, this implies roughly 10 to 30 iterations. From (3) it is obvious that the estimates of the effective temperatures may in principle be more uncertain the higher the value of  $\delta$ ; i.e. for the hottest stars. In Table 1 are listed the fractions  $\delta_{\text{UV}}$  and  $\delta_{\text{IR}}$  for different effective temperatures and gravities. As seen in this table,  $\delta$  has a low dependence on  $\log g$ .

### 3.2. Effective temperatures of B-type supergiants

The theoretical ASEDs predicted for supergiants by the wind-free plane-parallel model atmospheres with the effective temperatures issued directly from Eq. (1), do not always fit well to the observed ASEDs in the near- and far-UV. Generally, the predicted fluxes are higher than the observed ones in wavelengths  $\lambda \lesssim 2200 \text{ \AA}$ , while they are lower in the near-UV. For the obtained  $T_{\text{eff}}$  they yield somewhat larger Balmer discontinuities than those observed. This might be partially due to the plane-parallel approximation of model atmospheres that probably is not suited to the extended atmospheric layers of these stars, to an incomplete treatment of the spectral line formation in such diluted atmospheres, to the omission of the effects produced on the photosphere by the stellar winds (Abbott & Hummer 1985; Gabler et al. 1989; Smith et al. 2002; Morisset et al. 2004), and also to an insufficient line blocking in the model atmospheres, as discussed by Remie & Lamers (1981). Thus, to obtain the  $T_{\text{eff}}^f$  parameter of supergiants, we have slightly modified the use of relations (1) and (2) through the following iteration procedure:

- 1) Adopt approximate values of  $T_{\text{eff}}$  and  $\log g$ ;

**Table 1.** Far-UV and IR fractions of the unobserved bolometric flux as a function of  $T_{\text{eff}}$  and  $\log g$ , the function  $\Lambda(T_{\text{eff}}, \log g)$ , and temperatures  $T_{\text{eff}}^f$  as a function of  $T_{\text{eff}}(\gamma)$ .

$T_{\text{eff}}(\gamma)$	$\log g = 4.0$					$\log g = 3.0$					$\log g = 2.5$				
	$\delta_{UV}^*$	$\delta_{IR}^*$	$\Lambda[T_{\text{eff}}(\gamma), g]$	$\gamma$	$T_{\text{eff}}^f$	$\delta_{UV}^*$	$\delta_{IR}^*$	$\Lambda[T_{\text{eff}}(\gamma), g]$	$\gamma$	$T_{\text{eff}}^f$	$\delta_{UV}^*$	$\delta_{IR}^*$	$\Lambda[T_{\text{eff}}(\gamma), g]$	$\gamma$	$T_{\text{eff}}^f$
10000	0.023	0.059	0.024	1.5	9970	0.024	0.059	0.028	1.5	9970	0.023	0.059	0.029	1.5	9960
				2.0	9940				2.0	9930				2.0	9930
12500	0.105	0.034	0.088	1.5	12360	0.099	0.034	0.086	1.5	12360	0.093	0.034	0.081	1.5	12370
				2.0	12220				2.0	12220				2.0	12240
15000	0.230	0.022	0.152	1.5	14710	0.218	0.022	0.135	1.5	14740	0.202	0.022	0.122	1.5	14770
				2.0	14390				2.0	14470				2.0	14520
17500	0.386	0.016	0.182	1.5	17090	0.353	0.016	0.155	1.5	17150	0.318	0.016	0.134	1.5	17200
				2.0	16640				2.0	16780				2.0	16880
20000	0.552	0.012	0.194	1.5	19450	0.484	0.012	0.157	1.5	19600	0.450	0.012	0.135	1.5	19650
				2.0	18950				2.0	19160				2.0	19290
22500	0.706	0.009	0.191	1.5	21940	0.596	0.010	0.139	1.5	22090	0.546	0.010	0.109	1.5	22190
				2.0	21340				2.0	21670				2.0	21860
25000	0.843	0.008	0.178	1.5	24420	0.693	0.008	0.106	1.5	24670	0.635	0.008	0.071	1.5	24780
				2.0	23800				2.0	24310				2.0	24540
27500	0.955	0.007	0.153	1.5	26950	0.823	0.007	0.093	1.5	27180				1.5	27180
				2.0	26380				2.0	26840				2.0	26840
30000	1.060	0.006	0.126	1.5	29520	1.023	0.006	0.087	1.5	29670				1.5	29670
				2.0	29010				2.0	29330				2.0	29330
32500	1.241	0.005	0.109	1.5	32050				1.5	32050				1.5	32050
				2.0	31580				2.0	31580				2.0	31580
35000	1.539	0.004	0.103	1.5	34540				1.5	34540				1.5	34540
				2.0	34060				2.0	34060				2.0	34060

For  $\Lambda(T_{\text{eff}})$  and  $T_{\text{eff}}$  the temperature  $T_{\text{eff}}(\gamma)$  is simply the effective temperature written in the first column of the table.

Parameters  $\delta_{UV}^*$  and  $\delta_{IR}^*$  are values of  $\delta_{UV}$  and  $\delta_{IR}$  calculated with  $T_{\text{eff}}(\gamma)$  and fluxes  $F_{\lambda}[T_{\text{eff}}(\gamma), \log g]$ , which do not undergo the transformation given by Eq. 6. To calculate them we have used  $\lambda_a = 1380 \text{ \AA}$  and  $\lambda_b = 11084 \text{ \AA}$ . Note that  $T_{\text{eff}}^f = T_{\text{eff}}(\gamma = 1)$ .

2) Interpolate the model fluxes in the far-UV and IR for the adopted  $(T_{\text{eff}}, \log g)$  parameters;

3) Use a least square procedure to search for an enhancement parameter  $\gamma$  of the line blocking in the  $1400 \leq \lambda \leq 2150 \text{ \AA}$  wavelength interval, and correct the failure of the wind-free model fluxes used to fit the far-UV spectral region. The validity of  $\gamma$  is then extended to the entire  $0 \leq \lambda \leq 2150 \text{ \AA}$  spectral region. The empirical method used to calculate  $\gamma$  and to modify the line-blocking is explained in §3.2.1;

4) Define a new effective temperature,  $T_{\text{eff}}(\gamma)$ , to account for the lack of energy in the far-UV, produced by the increased absorption induced by  $\gamma$  and for the redistribution of this energy in the longer wavelengths. The calculation of  $T_{\text{eff}}(\gamma)$  is explained in §3.2.2;

5) Interpolate the model fluxes in the far-UV and IR for the  $T_{\text{eff}}(\gamma)$  and  $\log g = \log g[T_{\text{eff}}(\gamma), \beta]$  parameters;

6) Calculate the angular diameter  $\theta^f$  using Eq. (2) and the IR fluxes dependent on the  $[T_{\text{eff}}(\gamma), \log g(T_{\text{eff}}(\gamma), \beta)]$  pair of fundamental parameters. With the fluxes interpolated in step 5), calculate also the bolometric corrections  $\delta_{UV}$  and  $\delta_{IR}$  as indicated in Eq. (3). The bolometric correction  $\delta_{UV}$  is calculated using the  $\gamma$ -modified far-UV fluxes  $\tilde{F}_{\lambda}$  defined in §3.2.1 by Eq. (6), where  $T_{\text{eff}}$  is replaced by  $T_{\text{eff}}(\gamma)$ :

$$\delta_{UV} = \frac{\pi}{4} \theta^2 \frac{\int_0^{\lambda_a} \tilde{F}_{\lambda}[T_{\text{eff}}(\gamma), \log g(T_{\text{eff}}(\gamma), \beta)] d\lambda}{f_{\text{obs}}}; \quad (4)$$

7) Use  $\delta_{UV}$  and  $\delta_{IR}$ , and  $\theta^f$  derived in step 6) to calculate the bolometric flux  $f$  with relation (3) and obtain from Eq. (1) a new estimate of  $T_{\text{eff}}^f$ ;

8) Continue the iteration in step 3) by searching for a new enhancement parameter  $\gamma$  using the far-UV fluxes  $F_{\lambda}[T_{\text{eff}}(\gamma)]$  interpolated in step 5).

### 3.2.1. Modification of theoretical fluxes

Since we are not interested here in reproducing detailed energy distributions to fit the observed ones, but rather in estimating the integrated amount of the emitted energy over the whole spectrum, we use an empirical method to minimize the disagreement between the predicted and the observed far-UV energy distributions. However, the method is not able to simulate the consequences due to the presence of winds which become conspicuous in the extreme-UV (Smith et al. 2002). Nevertheless, this fact cannot significantly change the estimate of  $T_{\text{eff}}^f$ , as we shall see in §5.1.

Thus, we have proceeded in a similar way as previously attempted by Remie & Lamers (1981) and Zorec & Mercado-Ibanez (1987), i.e. we have modified the blocking degree of spectral lines in

the  $\lambda \lesssim 2150 \text{ \AA}$  region by writing the radiative flux emitted by a star at a given  $\lambda$  as:

$$F_\lambda(T_{\text{eff}}, \log g) = F_c(1 - b_\lambda), \quad (5)$$

where  $F_c$  is the continuum flux for a given set of parameters  $(T_{\text{eff}}, \log g)$ , and  $b_\lambda$  is the line blocking factor. The line blocking factor  $b_\lambda$  easily can be calculated using the  $F_\lambda$  and  $F_c$  fluxes listed by Castelli & Kurucz (2003) (<http://kurucz.harvard.edu/grids.html>). The enhanced line blocking factor was then calculated by multiplying  $b_\lambda$  by a parameter  $\gamma$ , which we assumed constant over all the wavelength interval  $0 \leq \lambda \leq 2150 \text{ \AA}$ . The modified theoretical flux at a given  $\lambda$  is then:

$$\tilde{F}_\lambda(T_{\text{eff}}, \log g) = F_\lambda(T_{\text{eff}}, \log g) \left( \frac{1 - \gamma b_\lambda}{1 - b_\lambda} \right). \quad (6)$$

For each star and at each iteration step of its  $T_{\text{eff}}^f$ , we looked for the value of  $\gamma$  that produced the best possible fit between the observed and theoretical fluxes, in the  $1400 \lesssim \lambda \lesssim 2150 \text{ \AA}$  wavelength interval. The model fluxes are calculated for a new effective temperature  $T_{\text{eff}}(\gamma)$ , which is different from  $T_{\text{eff}}^f$ , and for a  $\log g$ , which change as the iteration of the effective temperature continues.

### 3.2.2. Effective temperature $T_{\text{eff}}(\gamma)$ of models

It can readily be understood that the estimate of  $\delta_{\text{UV}}$  with the modified fluxes given by Eq. (6), where in most cases  $\gamma > 1$ , leads to an effective temperature lower than the nominal value,  $T_{\text{eff}}$ , of the model used. Thus, when using Eq. (6) in the wavelength range  $0 \leq \lambda \leq 2150 \text{ \AA}$ , we can recover the bolometric flux initially represented by the model characterized by  $(T_{\text{eff}}, \log g)$ , by means of a new effective temperature, named hereafter  $T_{\text{eff}}(\gamma)$ , which is larger than  $T_{\text{eff}}$  if  $\gamma > 1$ . Mathematically, this is due to the lack of energy produced by an increased absorption in the far-UV. Physically, this accounts for a redistribution of the excess of absorbed energy in the far- and extreme-UV, towards the near-UV, visible and IR spectral regions produced by the back-warming induced by the enhanced line blocking. To find the relation between  $T_{\text{eff}}$  and  $T_{\text{eff}}(\gamma)$ , we write the same bolometric flux,  $F_{\text{bol}}$ , in terms of both temperatures. On the one hand, it can be calculated using model fluxes dependent on  $T_{\text{eff}}$  as:

$$F_{\text{bol}} = \int_0^{\lambda_a} F_\lambda(T_{\text{eff}}) d\lambda + \int_{\lambda_a}^{\infty} F_\lambda(T_{\text{eff}}) d\lambda, \quad (7)$$

and, on the other hand, the same  $F_{\text{bol}}$  can be obtained with models that are a function of  $T_{\text{eff}}(\gamma)$ , as follows:

$$F_{\text{bol}} = \int_0^{\lambda_a} \tilde{F}_\lambda[T_{\text{eff}}(\gamma)] d\lambda + \int_{\lambda_a}^{\infty} F_\lambda[T_{\text{eff}}(\gamma)] d\lambda, \quad (8)$$

where  $\tilde{F}_\lambda[T_{\text{eff}}(\gamma)]$  is given by the relation (6). Since

$$F_{\text{bol}} = \frac{\sigma_R}{\pi} T_{\text{eff}}^4 \quad (9)$$

and

$$\frac{\sigma_R}{\pi} T_{\text{eff}}^4(\gamma) = \int_0^{\lambda_a} F_\lambda[T_{\text{eff}}(\gamma)] d\lambda + \int_{\lambda_a}^{\infty} F_\lambda[T_{\text{eff}}(\gamma)] d\lambda, \quad (10)$$

by subtracting (8) from (9) and this result from (10), we obtain the sought relation:

$$T_{\text{eff}}(\gamma)^4 = T_{\text{eff}}^4 + \left( \frac{\pi}{\sigma_R} \right) \int_0^{\lambda_a} \{ F_\lambda[T_{\text{eff}}(\gamma)] - \tilde{F}_\lambda[T_{\text{eff}}(\gamma)] \} d\lambda, \quad (11)$$

where we have not made explicit the dependence on  $\log g$ , but we have written that in the  $0 \lesssim \lambda \lesssim 2150 \text{ \AA}$  wavelength interval, the unmodified fluxes  $F_\lambda$  and modified fluxes  $\tilde{F}_\lambda$ , are both calculated for the effective temperature  $T_{\text{eff}}(\gamma)$ . It is obvious that to have the corresponding  $T_{\text{eff}}(\gamma)$  at each iteration step of the stellar effective temperature we put  $T_{\text{eff}} = T_{\text{eff}}^f$  and iterate the relation (11). Then, replacing Eq. (6) into (11), we derive:

$$T_{\text{eff}}^f = T_{\text{eff}}(\gamma) \left\{ 1 - (\gamma - 1) \Lambda[T_{\text{eff}}(\gamma), \log g] \right\}^{1/4}, \quad (12)$$

where the function  $\Lambda[T_{\text{eff}}(\gamma), \log g]$  is given by:

$$\Lambda[T_{\text{eff}}(\gamma), \log g] = \left( \frac{\pi}{\sigma_R} \right) \left[ \frac{\int_0^{\lambda_a} F_\lambda[T_{\text{eff}}(\gamma)] \left( \frac{b_\lambda}{1 - b_\lambda} \right) d\lambda}{T_{\text{eff}}^4(\gamma)} \right], \quad (13)$$

which can be calculated as a function of  $(T_{\text{eff}}, \log g)$  and used to derive the required value of  $\Lambda[T_{\text{eff}}(\gamma)]$  by interpolation. The function  $\Lambda[T_{\text{eff}}(\gamma), \log g]$  is given in Table 1, where we also give the values of  $T_{\text{eff}}^f$  derived from (12). In this table  $T_{\text{eff}}(\gamma)$  appears as the entering temperature. Actually, in the calculation of the stellar effective temperatures, we enter relation (12) with  $T_{\text{eff}}^f$  and deduce the corresponding value of  $T_{\text{eff}}(\gamma)$  at each iteration step. At each iteration step of  $T_{\text{eff}}^f$ , obtained by means of Eqs. (1) and (2), and  $\delta_{\text{UV}}$  calculated with (6), we changed the gravity parameter accordingly using the tables of  $\log g = \log g(\beta, T_{\text{eff}})$  given by Castelli & Kurucz (2006). For instance, in Fig. 1 we show the results obtained at the final step of the analysis carried out for HD 41117. For this particular star we have obtained  $T_{\text{eff}} = 20\,740 \text{ K}$ ,  $T_{\text{eff}}(\gamma) = 21\,100 \text{ K}$ ,  $\gamma = 1.53$  and  $\log g = 2.5$ . All fluxes in Fig. 1, observed and modelled, are normalized to a given flux in the visible wavelengths where the angular diameter is calculated. However, in the plot the logarithm of the fluxes is shifted by a constant value. We can also see that for  $T_{\text{eff}}^f$  and  $\gamma = 1.0$  the model fluxes in the far-UV are higher than the observed ones. In spite of the roughness of our approach, the fluxes from models computed with  $T_{\text{eff}}(\gamma)$  and  $\gamma = 1.53$  improve the fit of the observed energy distribution. It is also seen that the  $\gamma$ -modified flux is slightly higher in  $\lambda \geq 2200 \text{ \AA}$  than the fluxes calculated with  $T_{\text{eff}}^f$ , which leads to a smaller Balmer discontinuity as desired, i.e.  $D_{\text{obs}} = 0.050 \text{ dex}$ ,  $D[T_{\text{eff}}(\gamma)] = 0.065 \text{ dex}$ , while it is  $D(T_{\text{eff}}^f) = 0.074 \text{ dex}$ .

It is important to note that  $\gamma > 1$  produces a lowering of fluxes in the far- and extreme-UV, while the effect carried by the stellar wind on the photosphere, neglected here, increases the emitted fluxes (see Smith et al. (2002)). As we shall see in §5.1, this increase happens at global flux levels that may have an effect on the estimate of  $\delta_{\text{UV}}$  at effective temperatures higher than  $20\,000 \text{ K}$ , as shown in §5.1. In general, the values

of  $\delta_{UV}$  obtained with wind-free models can differ significantly from those derived with non-LTE BW models if  $\gamma \gtrsim 1.5$ . The variation of  $\delta_{UV}$  with  $\gamma$  can be obtained by noting that we can write:

$$\delta_{UV}(\gamma) = \frac{\int_0^{\lambda_a} \widetilde{F}_\lambda[T_{\text{eff}}(\gamma)]d\lambda}{\int_{\lambda_a}^{\lambda_b} F_\lambda[T_{\text{eff}}(\gamma)]d\lambda}, \quad (14)$$

where  $\widetilde{F}_\lambda$  is given by Eq. (6). We introduce the bolometric corrections  $\delta_{UV}^*$  and  $\delta_{IR}^*$  defined as:

$$\delta_{UV}^* = \frac{\int_0^{\lambda_a} F_\lambda[T_{\text{eff}}(\gamma)]d\lambda}{\int_{\lambda_a}^{\lambda_b} F_\lambda[T_{\text{eff}}(\gamma)]d\lambda}; \quad \delta_{IR}^* = \frac{\int_{\lambda_b}^{\infty} F_\lambda[T_{\text{eff}}(\gamma)]d\lambda}{\int_{\lambda_a}^{\lambda_b} F_\lambda[T_{\text{eff}}(\gamma)]d\lambda}, \quad (15)$$

which are written in terms of fluxes calculated for  $T_{\text{eff}}(\gamma)$  that do not undergo the transformation used for  $\widetilde{F}_\lambda$  in the far- and extreme-UV. Subtracting  $\delta_{UV}^*$  from (14) and taking into account the definition of  $T_{\text{eff}}(\gamma)$  written as:

$$\frac{\sigma_R}{\pi} T_{\text{eff}}^4(\gamma) = \int_{\lambda_a}^{\lambda_b} F_\lambda[T_{\text{eff}}(\gamma)]d\lambda \times (1 + \delta_{UV}^* + \delta_{IR}^*), \quad (16)$$

by making use of (13), we readily obtain:

$$\delta_{UV}(\gamma) = \delta_{UV}^* - (\gamma - 1)(1 + \delta_{UV}^* + \delta_{IR}^*) \times \Lambda[T_{\text{eff}}(\gamma), \log g], \quad (17)$$

where  $\delta_{UV}^*$ ,  $\delta_{IR}^*$  and the function  $\Lambda$  are given in Table 1.

In the visible wavelengths used to calculate the stellar angular diameter, the blocking factor is  $b_\lambda \sim 0$  and the enhancement parameter is reduced to  $\gamma = 1$ . However, the model fluxes employed to obtain  $\theta_\lambda$  in Eq. (2) are for the effective temperature  $T_{\text{eff}}(\gamma)$ , i.e.  $F_\lambda[T_{\text{eff}}(\gamma)]$ . In general, when  $\gamma \neq 1$  the effective temperature  $T_{\text{eff}}^f$  issued from (1) is higher than for  $\gamma = 1$ . Figure 2 shows  $\Delta T_{\text{eff}}^f = T_{\text{eff}}^f(\gamma \neq 1) - T_{\text{eff}}^f(\gamma = 1)$  for our sample of supergiants. Thus, even though  $\gamma$  can sometimes be as high as  $\gamma \sim 2$ , we see that the differences in the final value of  $T_{\text{eff}}^f$  are less than 300 K, which is much lower than the average expected error affecting the determination of  $T_{\text{eff}}^f$  (see §5). Finally, we note that for the stars in common with Remie & Lamers (1981), our  $\gamma$  values are systematically smaller by  $\Delta\gamma \sim 0.5$  than theirs, probably because in the models used here the line blocking effect is more realistic than in the Kurucz (1979) models.

## 4. The program stars and the observed quantities

### 4.1. BCD parameters

The program B-type stars, dwarfs to supergiants, are simply those for which both the BCD ( $\lambda_1, D$ ) parameters and calibrated fluxes from the far-UV to the IR, at least up to  $1\mu\text{m}$  were available. In this work we excluded stars with the Be phenomenon, but included some A0 to A2 type stars in the cold extreme of the hot fold of the BCD ( $\lambda_1, D$ ) diagram. The list of the program stars and their ( $\lambda_1, D$ ) are given in Table 2.

Our sample contains 217 stars with MK luminosity classes from V to Ia. Observations in the BCD system were carried out over different periods. Most of them were observed with

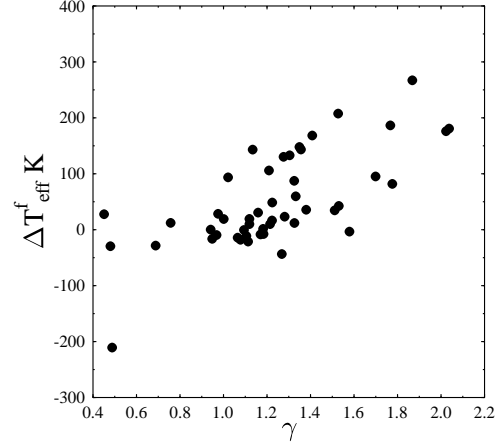


**Fig. 2.** Difference  $\Delta T_{\text{eff}}^f = T_{\text{eff}}^f(\gamma \neq 1) - T_{\text{eff}}^f(\gamma = 1)$  against  $\gamma$ .

the Chalonge spectrograph (Baillet et al. 1973) attached to several telescopes at the Haute Provence Observatory from 1977 to 1987 and at the ESO (La Silla) from 1978 to 1988. More recently, on January 2006, low resolution spectra in the optical wavelength range  $\lambda\lambda$  3400-5400 Å were obtained at CASLEO (Argentina), with the Boller & Chivens spectrograph. These spectra were wavelength and flux calibrated. Since the parameter  $\lambda_1$  depends on the spectral resolution, we selected a resolution of 7 Å at  $\lambda$  3760 Å, which is similar to the resolution required in the original BCD system. From the spectra obtained at CASLEO, the BCD ( $\lambda_1$  and  $D$ ) parameters were directly measured on the spectrograms. We have determined the parameter  $D = \log(F_{+3700}/F_{-3700})$  following the original BCD prescriptions (Chalonge & Divan 1952). We also controlled that  $F_{-3700}$  corresponds to the flux level where the higher members of Balmer lines merge. Most stars have been observed many times, so that for each star the adopted ( $\lambda_1, D$ ) set comes from 2 to about 50 determinations. The uncertainties that characterize these quantities are then  $\sigma_D \simeq 0.015$  dex and  $\sigma_{\lambda_1} \simeq 2\text{Å}$ , respectively.

### 4.2. ASED data

The ASED data were collected in the CDS astronomical database. The far-UV fluxes used in this work were obtained with the IUE spectra in low resolution mode and the 59 narrow-band fluxes, between 1380 and 2500 Å measured during the S2/68 experiment from the TD1 satellite (Jamar et al. 1976; Macau-Hercot et al. 1978). We have compared the TD1 fluxes with the low resolution IUE spectra calibrated in absolute fluxes, but we have not detected any systematic deviation neither in the far-UV ASED nor in the values of  $f$  obtained. The TD1 fluxes give a homogeneous far-UV flux data set, for they are laboratory based calibrations.

In the visible and near-IR spectral region, fluxes are from Breger's catalogue (Breger 1976a,b) and the 13-color photometry calibrated in absolute fluxes (Johnson & Mitchell 1975) (hereinafter JM). The normalized 13-color fluxes of the stars in common were compared to Breger (1976a,b) spectrophotome-

try and to the monochromatic fluxes observed by Tüg (1980). The comparison of JM's absolute fluxes with those of known flux standards  $\alpha$  Lyr (HD 172167), 109 Vir (HD 130109) and  $\eta$  UMa (HD 120315) given in the Hayes & Latham (1975) system revealed no noticeable differences in the  $\lambda\lambda 0.58\text{-}0.80\ \mu\text{m}$  spectral region, which was chosen in this work to obtain the stellar angular diameter  $\theta^f$ . Nevertheless, there are small differences near the BD that lie within the uncertainties of other calibrations, but they do not affect the estimate of  $f$ . We also noticed that JM's fluxes give consistent continuations to the IUE and ANS fluxes (Wesseliuss et al. 1982).

### 4.3. Correction for interstellar extinction

The adopted ISM extinction law is from Cardelli et al. (1989) and O'Donnell (1993). The ratio  $R_V = A_V/E(B - V)$  was adopted in this work according to the galactic region, as specified in Gulati et al. (1987) and Gulati et al. (1989). The adopted color excess  $E(B - V)$  is the average of several more or less independent determinations based on the following methods: a) UBV photometry with the standard intrinsic colors given by Lang (1992); b) BCD system with the intrinsic gradients  $\Phi_{rb}^o$  taken from the calibration done by Chalonge & Divan (1973) from where we obtain that  $E(B - V) = 0.55[\Phi_{rb}^o - \Phi_{rb}^o]$ ; c) depths of the 2200 Å ISM absorption band (Beeckmans & Hubert-Delplace 1980; Zorec & Briot 1985); d) profile parameters of the 2200 Å band (Guertler et al. 1982; Friedemann et al. 1983; Friedemann & Roeder 1987) calibrated in  $E(B - V)$  (Moujtahid 1993); e) diagrams of  $E(B - V)$  vs. distance obtained with 'normal' stars surrounding the program stars within less than  $2^\circ$ . The UBV photometry used is from the CDS compilation and the distances are either from the HIPPARCOS satellite or spectroscopy.

### 4.4. Results

The list of the program stars is given in Table 2: 1) HD number of the star; 2) the MK SpT/LC determined with the BCD system; 3) the parameter  $\lambda_1$  in  $\lambda_1 - 3700\ \text{Å}$ ; 4) the Balmer discontinuity  $D$  in dex; 5) the adopted average color excess  $E(B - V)$ , in mag; 6) the effective temperature  $T_{\text{eff}}^f$  with its estimated uncertainty, given in K; 7) the angular diameter with its estimated uncertainty, given in mas (milliarcseconds); 8) the parameter  $\gamma$  used to fit the observed far-UV ASSED (see §3.2); 9) the  $T_{\text{eff}}(\lambda_1, D)$  read on the new calibration curves (see Fig. 10a).

## 5. Comments on the uncertainties affecting the $T_{\text{eff}}^f$ and $\theta^f$ determinations

### 5.1. Systematic deviations

Hot supergiants have massive winds whose optical depths can be high enough to heat somewhat the photosphere back to the continuum formation region. Thus, both spectral lines and the emitted continuum energy distribution can in principle be modified (Abbott & Hummer 1985; Gabler et al. 1989; Smith et al.

2002; Morisset et al. 2004). Since the models used in this work are wind-free, doubts can be raised about whether the use of these models introduces systematic effects on the estimate of  $T_{\text{eff}}^f$ . As is seen in §6, this question may be of particular interest at  $T_{\text{eff}} = 25\ 000\ \text{K}$ . We then compared the absolute energy distribution produced by a non-LTE BW model atmosphere for supergiants (Smith et al. 2002) with that predicted by an LTE wind-free model atmosphere for  $T_{\text{eff}} = 25\ 000\ \text{K}$  and  $\log g = 2.95$ , similar to those used in the present work (Castelli & Kurucz 2003). This comparison is shown in Fig. 3 where we see [Fig. 3(a)] that the most significant differences appear only in the extreme-UV energy distribution, at  $\lambda \lesssim 500\ \text{Å}$ . In this spectral region the fluxes are between two and three orders of magnitude lower than in slightly longer wavelengths, where the most significant contribution to the value of the filling factor  $\delta_{\text{UV}}$  in relation (3) arises. Although the differences seen in  $\lambda \lesssim 500\ \text{Å}$  can certainly be important for the excitation/ionization of the stellar environment, as we shall see below, they seem to have a limited incidence on the estimate of the stellar bolometric flux  $f$  on which the estimate of  $T_{\text{eff}}^f$  relies.

In Fig. 3(b) we also see that the fluxes produced by both types of models are similar in the visible wavelengths where the angular diameter  $\theta^f$  is calculated. This ensures that  $\theta^f$  does not suffer from the use of plane-parallel model atmospheres either. The same conclusion is reached from Fig. 5 by comparing the obtained  $\theta^f$  values with the measured angular diameters.

Let us now explore what systematic deviation can be expected in our  $T_{\text{eff}}^f$  estimates due to the use of fluxes predicted by wind-free models of stellar atmospheres. In what follows, we use the notation  $T_{\text{eff}}^{f,w}$  and  $\delta_{\text{UV,IR}}^w$  to designate the parameters that should be derived with non-LTE BW model atmospheres. In §6.1 and Fig. 5 it is demonstrated that the angular diameters  $\theta^f$  obtained agree well with the observed ones. This means that they cannot introduce a systematic deviation in the derivation of  $T_{\text{eff}}^f$  with Eq. (1). Then, the ratio between  $T_{\text{eff}}^{f,w}$  and  $T_{\text{eff}}^f$  is given by:

$$\frac{T_{\text{eff}}^{f,w}}{T_{\text{eff}}^f} = \frac{1 + \delta_{\text{UV}}^w + \delta_{\text{IR}}^w}{1 + \delta_{\text{UV}}(\gamma) + \delta_{\text{IR}}(\gamma)}, \quad (18)$$

where  $\delta_{\text{UV}}(\gamma)$  and  $\delta_{\text{IR}}(\gamma)$  are the bolometric corrections calculated with wind-free models for different values of the enhancement parameter  $\gamma$ . The value of  $\delta_{\text{UV}}(\gamma)$  is obtained from Eq. (17), while it is reasonable to assume that  $\delta_{\text{IR}}^w \approx \delta_{\text{IR}}(\gamma) = \delta_{\text{IR}}^*$ . Concerning the non-LTE BW model  $\delta_{\text{UV}}^w$  bolometric correction, we ask what extreme-UV flux excess carried by the wind-related effects must exist to explain the underestimations suggested by the comparison shown in Fig. 7 that possibly affect our  $T_{\text{eff}}^f$  determinations for supergiants. To this end we simply write:

$$\delta_{\text{UV}}(w) = w \times \delta_{\text{UV}}^*, \quad (19)$$

where the factor  $w$  mimics the extreme-UV flux excess due to wind-related effects. Using for  $\delta_{\text{UV,IR}}^*$  and  $\Lambda(T_{\text{eff}}, \log g)$  the values given in Table 1, we readily obtain the estimates of  $w$  for a series of imposed underestimations  $\Delta T_{\text{eff}}^f$  which are displayed in Table 3.

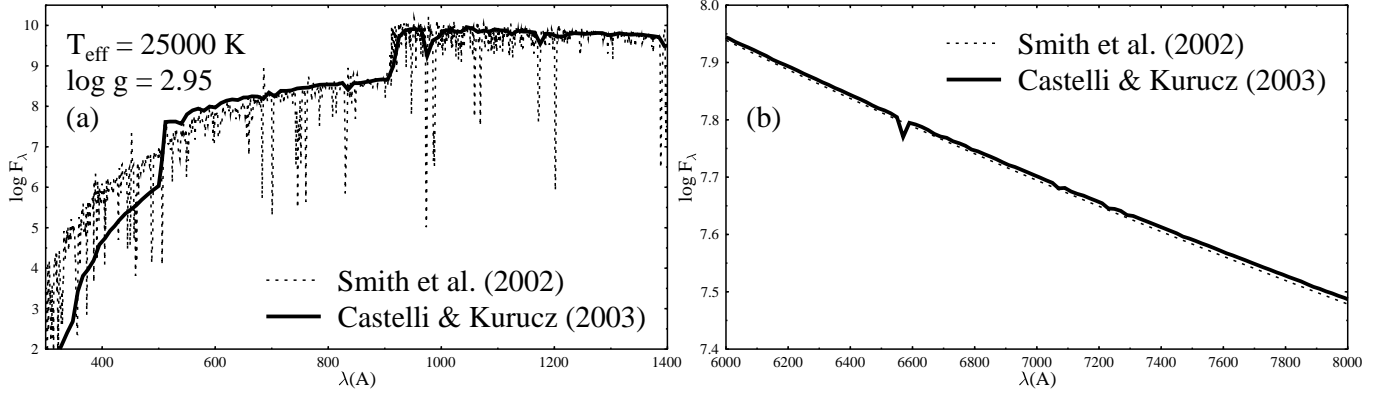


**Fig. 3.** Comparison of theoretical ASEDs from non-LTE blanketed model atmospheres with stellar winds for  $T_{\text{eff}} = 25\,000\text{ K}$  and  $\log g = 2.95$  calculated by Smith et al. (2002) (dotted line), with LTE wind-free models obtained by Castelli & Kurucz (2003) (full line).

**Table 3.** Extreme-UV flux excess factors  $w$  as a function of the effective temperature and  $\gamma$ , needed to explain the  $\Delta T_{\text{eff}}^f$  underestimations affecting the  $T_{\text{eff}}^f$  values for supergiants.

$T_{\text{eff}}$ K	$\Delta T_{\text{eff}}^f$ K	$w(\gamma)$		
		$\gamma = 1.0$	$\gamma = 1.5$	$\gamma = 2.0$
10000	-500	10.73	9.96	9.19
	-1000	21.94	21.02	20.09
	-1500	34.80	33.69	32.59
	-2000	49.45	48.14	46.83
15000	-500	1.78	1.36	0.92
	-1000	2.68	2.18	1.68
	-1500	3.64	3.08	2.52
	-2000	4.70	4.06	3.43
20000	-500	1.32	1.05	0.79
	-1000	1.67	1.37	1.08
	-1500	2.04	1.71	1.39
	-2000	2.43	2.08	1.72
25000	-500	1.20	1.06	0.92
	-1000	1.41	1.27	1.11
	-1500	1.64	1.48	1.32
	-2000	1.89	1.71	1.53
30000	-500	1.14	1.04	0.95
	-1000	1.28	1.18	1.08
	-1500	1.43	1.32	1.22
	-2000	1.59	1.47	1.36

The estimates are done for  $\log g = 3.0$

From the non-LTE BW models published by Smith et al. (2002) we obtain,

$$\begin{aligned} w(25\,000, 2.95) &= 1.05 \\ w(30\,200, 3.14) &\simeq 1.08 \end{aligned} \quad (20)$$

for  $T_{\text{eff}} = 25\,000\text{ K}$ ,  $\log g = 2.95$  and  $T_{\text{eff}} = 32\,200\text{ K}$ ,  $\log g = 3.14$ , respectively, where  $T_{\text{eff}} = 25\,000\text{ K}$  corresponds to the

effective temperature where there are strong deviations in the diagram of Fig. 7. Unfortunately Smith et al. (2002) have not made available fluxes for  $T_{\text{eff}} < 25\,000\text{ K}$ . Then, by extrapolation and approximate calculation with our codes for extended spherical atmospheres (Cruzado et al. 2007), we get the value  $w(20\,000, 3.0) \simeq 1.04$ . The values of  $w$  derived here are close to those in Table 3 for  $\gamma = 1.5$ . Since for the supergiants that are in common with those in the  $T_{\text{eff}}^{(6)}$  category (see §6.2), we have  $\gamma \lesssim 1.5$ , it means that we may expect our  $T_{\text{eff}}^f$  to be systematically smaller by less than 470 K, 480 K and 640 K, for objects whose temperatures are 20 000 K, 25 000 K and 30 000 K, respectively. In addition, for later B sub-spectral types, the underestimates can be even smaller, as it is difficult to believe that the  $w$  parameters are larger than those quoted above when  $T_{\text{eff}} < 20\,000\text{ K}$ . For  $\gamma \simeq 2$  (see Table 3) differences easily can approach 1 000 K. Nevertheless, there is only one common late type supergiant with  $\gamma > 1.5$  (HD 202850,  $\gamma = 1.78$ ), for which curiously the difference between our estimate and that in the  $T_{\text{eff}}^{(6)}$  group is +170 K. We note that to obtain the imposed underestimation  $\Delta T_{\text{eff}}^f$  when  $w < 1$  for a given factor  $\gamma$ , the non-LTE BW models should predict lower extreme-UV fluxes than wind-free models do.

The model atmospheres used in this work to obtain  $T_{\text{eff}}^f$  are interpolated here for  $\log g$  parameters that were estimated using the uvby- $\beta$  photometry. As the index  $\beta$  is calibrated mainly for dwarf and giant stars, to see whether its extrapolation induces significant systematic effect for supergiants, we compare in Fig. 4 the  $\log g(\beta)$  adopted in the present work, with the  $\log g(\text{lines})$  parameters derived in the literature by detailed fitting of spectral lines with model atmospheres, mainly hydrogen H $\gamma$  and H $\delta$  lines (McErlean et al. 1999; Repolust et al. 2004; Martins et al. 2005; Crowther et al. 2006; Benaglia et al. 2007; Markova & Puls 2008; Searle et al. 2008). From this comparison we can conclude that our estimates of  $\log g$  do not deviate either strongly or in a systematic way from those based on spectral lines. Although in the cited works the authors claim that their  $\log g(\text{lines})$  are determined with errors ranging from 0.10 to 0.15 dex, they differ among them by 0.10 to 0.29 dex. The comparison in Fig. 4 of our  $\log g(\beta)$  estimates with  $\log g(\text{lines})$

shows that most of the points deviate randomly from the first diagonal within 0.25 dex. This implies that we do not expect that the  $\log g(\beta)$  values used in the present work will induce systematic errors in the  $T_{\text{eff}}^f$  and  $\theta^f$  parameters.

In conclusion, we do not see how we can attribute to our BFM method systematic effective temperature deviations attaining 2 000 K, or more than 5 000 K, as observed in Fig. 7.

## 5.2. Random errors

The  $T_{\text{eff}}^f$  values issued from relation (1) and the  $\theta^f$  parameters derived with Eq. (2) have the following sources of error: a) the ISM color excess  $E(B - V)$ ; b) the line blocking enhancement parameter  $\gamma$ ; c) the  $\log g$  parameter on which depend the model fluxes used to estimate the angular diameter and the filling factor due to the unobserved spectral region; d) the filling factor  $\delta$  used to calculate the bolometric flux in relation (3).

In Appendix §B we explain in detail how we have calculated the uncertainties of  $T_{\text{eff}}^f$  and  $\theta^f$  by taking into account the combined effect of all error sources mentioned above. Since the most important uncertainty on  $T_{\text{eff}}^f$  and  $\theta^f$  is produced by the error on the ISM color excess estimate  $E(B - V)$ , in this section we consider only the effect caused by this parameter as if it were the sole error source. Let us recall that the  $E(B - V)$  affects the bolometric flux estimate through  $f_{\text{obs}}$  in (3) of §3.1, and the monochromatic fluxes on which the calculation of the stellar angular diameter depends. However, from (1) and (2) we find that:

$$T_{\text{eff}}^f \propto (f/f_\lambda)^{1/4} \quad (21)$$

which implies that the effect on the estimate of  $T_{\text{eff}}^f$  by an error on  $E(B - V)$  is reduced by the error of the monochromatic fluxes entering the calculation of  $\theta^f$ . In Table 4 are given the estimates of the errors produced on  $T_{\text{eff}}^f$  and  $\theta^f$  by the uncertainty  $\Delta E(B - V)$  in the ISM color excess, assuming that it is the only source of error. We note the asymmetric propagation of uncertainties in  $T_{\text{eff}}^f$  and  $\theta^f$  due to those in  $E(B - V)$ . Since for us  $\Delta E(B - V) \lesssim 0.03$ , from Table 4 we find that on average the corresponding errors are of 5% in  $T_{\text{eff}}^f$  and 2% in  $\theta^f$ .

## 6. Comparison with other $\theta$ and $T_{\text{eff}}$ determinations

### 6.1. Apparent angular diameters

In spite of the fact that for the wavelengths where  $\theta^f$  is calculated, all models predict roughly the same flux level, the angular diameter is in principle the quantity among those estimated in this work that can be the most strongly model-dependent. To test our angular diameter determinations, we have compared them with those found in the literature. We used the data collected in Pasinetti Fracassini et al. (2001), where we discarded the very old determinations and privileged those determined by interferometry. The comparison is shown in Fig. 5, where we put on the ordinate axis the average values from the data in Pasinetti Fracassini et al. (2001) and the respective  $1\sigma$  error bars. In this figure we can see that there is no systematic deviation of points from the first bisecting line and that they distribute around it with a fairly uniform dispersion:  $\sigma_\theta = 0.045$

**Table 4.** Uncertainties on  $T_{\text{eff}}^f$  and  $\theta^f$  as a function of  $T_{\text{eff}}$  and  $\log g$  due to errors in the estimate of the ISM color excess  $E(B - V)$ .

$T_{\text{eff}}$ K	$\Delta T_{\text{eff}}^f / T_{\text{eff}}^f$				$\Delta \theta / \theta^f$			
	$\Delta E(B - V)$ mag				$\Delta E(B - V)$ mag			
	-0.07	-0.03	0.03	0.07	-0.07	-0.03	0.03	0.07
	$\log g = 4.5$							
10000	-0.054	-0.025	0.027	0.067	-0.054	-0.023	0.023	0.054
15000	-0.087	-0.040	0.043	0.106	-0.041	-0.017	0.017	0.039
20000	-0.100	-0.045	0.049	0.120	-0.036	-0.015	0.015	0.034
25000	-0.107	-0.048	0.052	0.127	-0.033	-0.014	0.014	0.032
30000	-0.111	-0.050	0.054	0.132	-0.031	-0.013	0.013	0.030
	$\log g = 3.5$							
10000	-0.050	-0.023	0.025	0.062	-0.052	-0.022	0.022	0.051
15000	-0.081	-0.037	0.040	0.098	-0.038	-0.016	0.015	0.035
20000	-0.093	-0.042	0.045	0.111	-0.032	-0.013	0.013	0.029
25000	-0.100	-0.045	0.048	0.117	-0.028	-0.012	0.012	0.026
30000	-0.104	-0.046	0.050	0.121	-0.027	-0.011	0.011	0.025
	$\log g = 2.5$							
10000	-0.059	-0.027	0.030	0.073	-0.056	-0.024	0.024	0.055
15000	-0.094	-0.043	0.047	0.116	-0.044	-0.018	0.018	0.042
20000	-0.108	-0.049	0.053	0.131	-0.039	-0.016	0.016	0.037
25000	-0.116	-0.052	0.057	0.139	-0.036	-0.015	0.015	0.035
30000	-0.120	-0.054	0.059	0.144	-0.034	-0.015	0.014	0.034

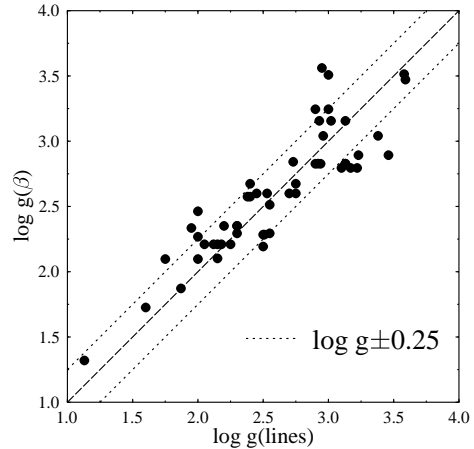


**Fig. 4.** Comparison of  $\log g(\beta)$  parameters used in this work and derived with the uvby- $\beta$  photometry, with those for the common supergiant stars estimated by other authors through spectral line fitting with model atmospheres.

mas. The uncertainty that can affect the  $T_{\text{eff}}^f$  values due to errors in the angular diameter estimates ranges then from  $\Delta T_{\text{eff}}^f / T_{\text{eff}}^f = 1.5\%$  to  $9\%$  as the angular diameter goes from  $\theta = 3.0$  mas to  $\theta = 0.5$  mas.

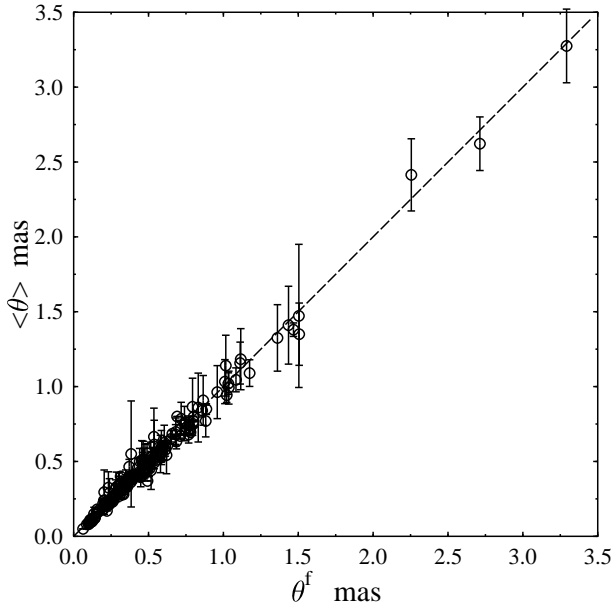


**Fig. 5.** Average apparent angular diameters  $\langle\theta\rangle$  in mas of our program stars determined by other authors (ordinates) against  $\theta^f$  obtained in the present work (abscissa).

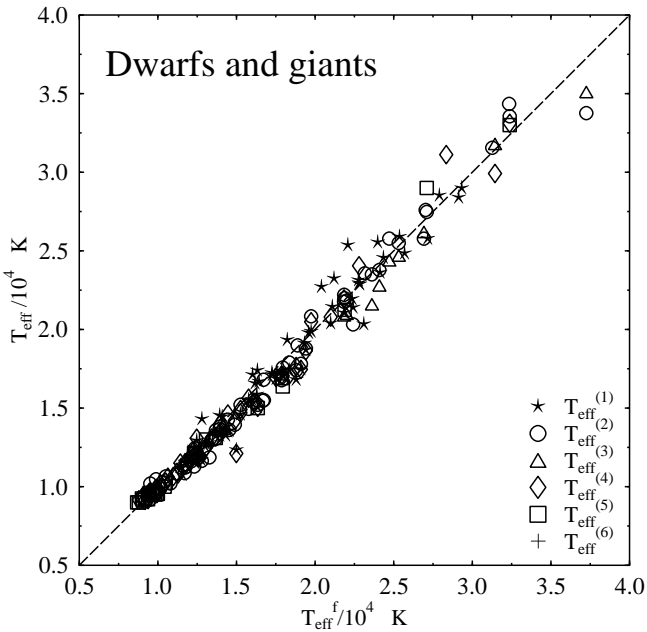


**Fig. 6.** Effective temperatures of dwarfs and giants determined by other authors (ordinates) against the  $T_{\text{eff}}^f$  estimates obtained in the present work (abscissa).

### 6.2. Effective temperatures

In order to test the accuracy of the effective temperatures obtained with the BFM method, we compared our values to those found in the literature. The  $T_{\text{eff}}$  values were gathered according to the method used to determine them:

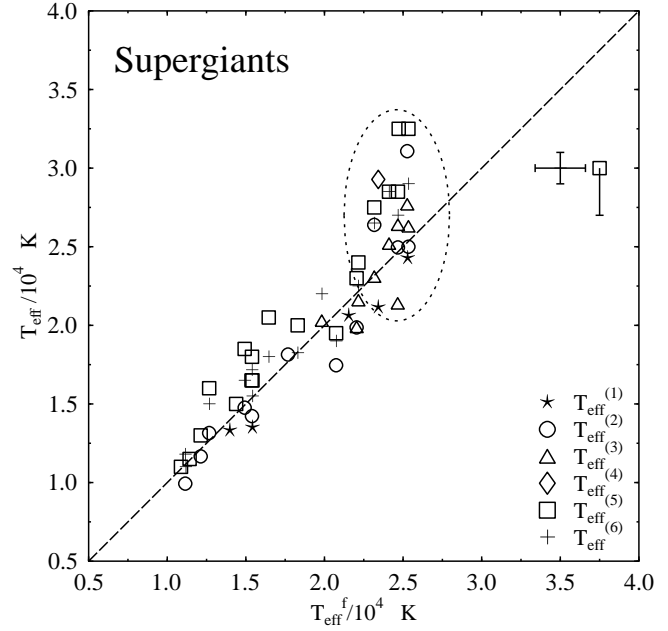


**Fig. 7.** Effective temperatures of supergiant stars determined by other authors (ordinates) against the  $T_{\text{eff}}^f$  estimates obtained in the present work (abscissa). The error bars correspond to temperatures inside the ellipse taken from Crowther et al. (2006)(vertical) and in the present work (horizontal). The square with a downward error bar indicates the systematic average shift that the McErlean et al. (1999) data might have.

- 1) The temperature is derived empirically using either the reddening-free color index QUV, as in Gulati et al. (1989), or the  $c_0$  and  $\beta$  indices of the Strömberg uvby- $\beta$  photometry (Castelli 1991).
- 2) The temperature is determined from integration of fluxes over a large interval of wavelengths, as was done by Code et al. (1976); Underhill et al. (1979); Malagnini et al. (1986).
- 3) The temperature is obtained by means of the BFM by Remie & Lamers (1981).
- 4) The temperature is evaluated by comparing the observed visual or UV fluxes with predictions from line-blanketed LTE model atmospheres, as in Malagnini et al. (1983); Morossi & Malagnini (1985); Malagnini & Morossi (1990).
- 5) The temperature is computed by means of: a) NLTE line-blanketed model analysis of ionization balances due to He I/II, Si III/IV and Si II/III on moderate resolution spectra, as done by McErlean et al. (1999) using the code TLUSTY (Hubeny 1988), or b) LTE line-blanketed model fitting of the optical region and H $\gamma$  profile using ATLAS9 model atmospheres as in Adelman et al. (2002).
- 6) The temperature is determined from synthetic fits to the optical spectral range of B supergiants employing unified NLTE line- and non-LTE BW extended model atmosphere codes, such as FASTWIND (Puls et al. 2005) or CMFGEN (Hillier et al. 2003), as in Searle et al. (2008); Markova & Puls (2008); Crowther et al. (2006).

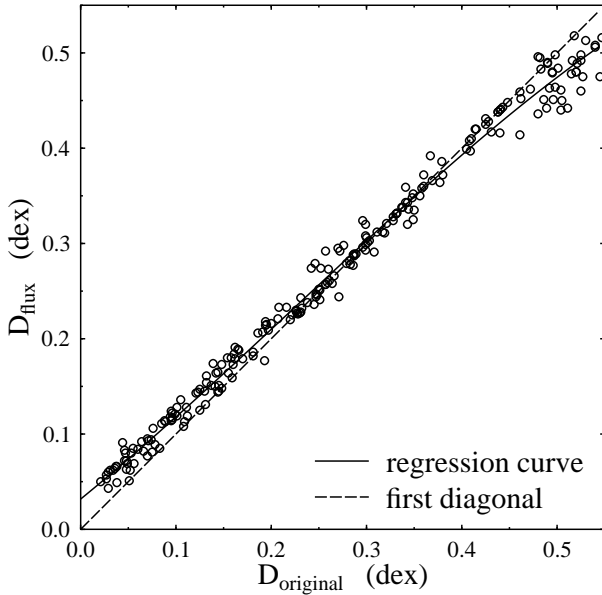


**Fig. 8.** Comparison between the original BCD Balmer discontinuities of the program stars (abscissa) and those determined with absolute flux-calibrated energy distributions (ordinates).

For each program star, Table 5 lists our determinations of  $T_{\text{eff}}^f$  together with the corresponding uncertainties and, in the following columns, the  $T_{\text{eff}}^{(i)}$  ( $i = 1, \dots, 6$ ) obtained by other authors with the methods described in items: 1) to 6). When more than one determination of  $T_{\text{eff}}$  exists for the same star, obtained using similar techniques, we adopted the mean value.

The difficulties in determining  $T_{\text{eff}}$  can be better shown by separating dwarfs and giants from supergiants. Figure 6 displays the comparison of  $T_{\text{eff}}^{(1)}$  (stars),  $T_{\text{eff}}^{(2)}$  (open circles),  $T_{\text{eff}}^{(3)}$  (open triangles),  $T_{\text{eff}}^{(4)}$  (diamonds),  $T_{\text{eff}}^{(5)}$  (open squares), and  $T_{\text{eff}}^{(6)}$  (plus signs) with our  $T_{\text{eff}}^f$  values (abscissa) for dwarfs and giants. From this figure, we can see that the differences in the  $T_{\text{eff}}$  estimates seem to be related to the absolute value of temperatures rather than to the adopted techniques. For  $T_{\text{eff}} \lesssim 20\,000$  K, all methods produce temperatures within  $\sigma_{T_{\text{eff}}} = 750$  K, while for  $T_{\text{eff}} \gtrsim 20\,000$  K,  $\sigma_{T_{\text{eff}}} = 1\,300$  K. We notice, however, that the  $T_{\text{eff}}$  derived with the BFM agree best with those obtained using line-blanketed LTE model atmospheres (Malagnini et al. 1983; Morossi & Malagnini 1985; Malagnini & Morossi 1990).

The same type of comparison, but for supergiants, is shown in Fig. 7 which appears less ordered than the plot for dwarfs and giants. However, the  $T_{\text{eff}}^{(5)}$  values do deviate strongly and in a systematic way. The  $T_{\text{eff}}^{(5)}$  values for supergiants are taken only from McErlean et al. (1999), and they were obtained with non-LTE wind-free model atmospheres. The observed deviations form a kind of ‘temperature-step’ rising at  $T_{\text{eff}} \sim 15\,000$  K and  $T_{\text{eff}} \sim 25\,000$  K, i.e. at temperatures identified as specific to the bi-stability phenomenon (Lamers et al. 1995; Vink et al. 1999; Crowther et al. 2006; Markova & Puls 2008). This fact may reveal that there can be effects related to the presence of

stellar winds which have not been taken into account in their models. Moreover, the noted deviations also reveal a dependence on the method used to determine the effective temperature. The  $T_{\text{eff}}$  values from McErlean et al. (1999) determined by He II line profile fits deviate on average from our temperatures by  $\langle \Delta T_{\text{eff}} \rangle = 5\,500 \pm 1\,800$  K at abscissa  $\langle T_{\text{eff}} \rangle = 24\,400 \pm 800$  K; the temperatures determined by the Si III/Si IV ionization balance deviate by  $\langle \Delta T_{\text{eff}} \rangle = 1\,300 \pm 380$  K at  $\langle T_{\text{eff}} \rangle = 20\,400 \pm 1\,900$  K; those determined from the Si II/Si III ionization balance deviate by  $\langle \Delta T_{\text{eff}} \rangle = 2\,200 \pm 1\,400$  K at  $\langle T_{\text{eff}} \rangle = 14\,600 \pm 1\,500$  K. The  $T_{\text{eff}}$  values from McErlean et al. (1999) have random errors  $\pm 1\,000$  K. McErlean et al. (1999) pointed out that their effective temperatures could in fact be 10% lower, which means that for the stars lying in the ellipse of Fig. 7 the temperatures are on average 3 000 K too high. Thus, excluding the  $T_{\text{eff}}^{(5)}$  values, the average dispersions with the remaining sources cited in Fig. 7 are  $\sigma_{T_{\text{eff}}} = 1\,250$  K for  $T_{\text{eff}} \lesssim 20\,000$  K, and  $\sigma_{T_{\text{eff}}} = 2\,800$  K for  $T_{\text{eff}} \gtrsim 20\,000$  K.

Stars in the  $T_{\text{eff}}^{(6)}$  group are from several sources, but their temperatures were derived using the same models, although corresponding to different implementation generations. Crowther et al. (2006) note that the current non-LTE BW model atmospheres lead to lower effective temperatures by 1 000 to 2 000 K, as compared to some earlier determinations in Kudritzki et al. (1999); Crowther et al. (2002); Repolust et al. (2004), and that their latest effective temperature estimates have uncertainties of about 1 000 K. However, three of the stars lying in the ellipse of Fig. 7: HD 30614, HD 37128 and HD 38771, were assigned temperatures that are from 2 300 K to 3 700 K higher than those obtained in the present work. From the discussion in Sect. 5.1 it appears that our method of determining the effective temperature does not introduce systematic deviations larger than 500 K to 700 K as the effective temperature goes from 20 000 K to 30 000 K. We suspect then that the spectral lines used to derive some  $T_{\text{eff}}^{(6)}$  may still undergo a perturbation that the existing non-LTE BW model atmospheres do not account for entirely. Among the phenomena that may explain the perturbed lines are: non-isothermal multicomponent plasma effects (Springmann & Pauldrach 1992), shocks and/or the presence of exo-photospheric density clumps. Regarding the latter, it is worth noting that the use of an average continuous stellar wind to mask a possible clumpy environment, where a mass-loaded wind must appear (Hartquist et al. 1986), can lead to misleading conclusions. The radiation transfer effects expected from the resulting average opacity are quite different from those the clumpy environment is able to produce (Boisse 1990). Furthermore, the actual opacity of the medium is higher than that expected from line diagnostic and the back warming on the photospheric layers could have different characteristics than those expected from winds with regular density and temperature structures.

## 7. Calibration of the $(\lambda_1, D)$ parameters into $T_{\text{eff}}$

### 7.1. The scale of the Balmer discontinuities

In the original BCD system, the Balmer discontinuities were obtained by comparing newly observed stars with stars ob-

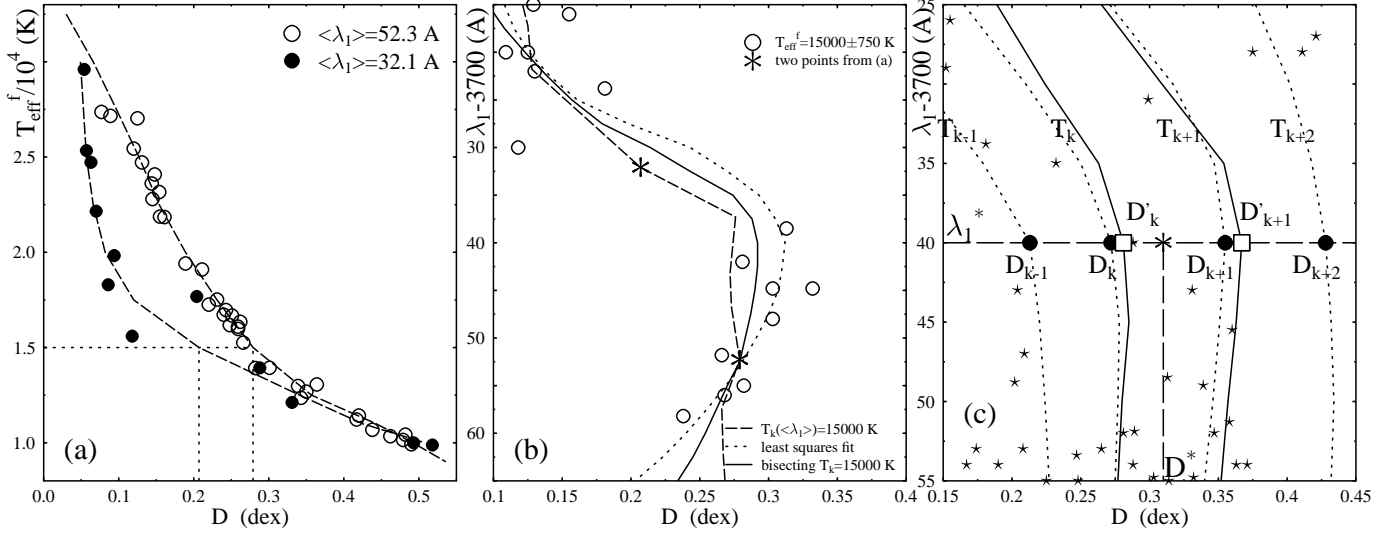


**Fig. 9.** The iteration of  $T_k = \text{constant}$  curves in the plane  $(\lambda_1, D)$ . a)  $T_{\text{eff}}^f = T_{\text{eff}}^f(D)$  relations for stars in strips of total width  $\Delta\lambda_1 = 10 \text{ \AA}$  and average  $\langle\lambda_1 - 3700\rangle = 32.1$  and  $52.3 \text{ \AA}$ . b) Bisection  $\lambda_1 = \lambda_1(D)$  curve for  $\overline{T}_k = 15\,000 \text{ K}$  (full line), between the  $\lambda_1 = \lambda_1(D|\overline{T}_k)$  obtained from panel a) (dashed curve) and the similar one derived by a least squares fit of a polynomial passing through stars in the plane  $(\lambda_1, D)$  having effective temperatures  $\overline{T}_k \pm \Delta T_k$  (dotted curve). c) Iterated correction of the  $T_{\text{eff}} = T_{\text{eff}}(\lambda_1, D) = \text{const.}$  layout.  $(\lambda_1^*, D^*)$  = coordinates of a test star.  $\bullet$  = abscissa of intersections between the  $\lambda_1^* = \text{constant}$  line and the  $T_k = \text{constant}$  curves at iteration step “n”;  $\square$  = abscissa of intersections between the  $\lambda_1^* = \text{constant}$  line and the new  $T_k = \text{constant}$  curves at iteration step “n+1”;  $\star$  = program stars.

served simultaneously for which  $D$  was known. The ‘zero’ of these  $D$  values was known within an uncertainty of some 0.012 dex (L. Divan, private communication). Conversely, for our program stars, we have derived the BD using absolute calibrated fluxes, and compared them with those determined in the original BCD system. The result is shown in Fig. 8. In this figure we can see that, on average, the deviation between both types of BD determinations amounts to the expected 0.012 dex in the region of early sub-spectral types, but that the difference is actually a function of  $D$ . The least-square fitted relation between the ‘old’ and ‘new’ BDs valid for the  $0.03 < D < 0.55$  dex interval is given by :

$$D_{\text{new}} = 0.032 + 0.817 \times D_{\text{old}} + 0.524 \times D_{\text{old}}^2 - 0.775 \times D_{\text{old}}^3, \quad (22)$$

where the  $D$  are given in dex. Therefore, in this work we used the scale of BDs determined from absolute fluxes, which enable the measured Balmer discontinuities to be directly compared with models. All diagrams in the present work are also given in the flux-calibrated  $D$ -scale.

## 7.2. The calibration

A calibration of the  $(\lambda_1, D)$  parameters into effective temperatures for dwarf to giant B-type stars has been presented in Divan & Zorec (1982). In the present work, we are mainly interested in extending the BCD calibration for B supergiants. To ensure a better consistency of the layout of iso-effective temperature curves, we need to calibrate the entire region in the bi-folded BCD  $(\lambda_1, D)$  surface that corresponds to OB-type stars of all luminosity classes. So, the iso-effective temperature curves for stars earlier than A2 of all luminosity classes are

obtained in two successive steps: 1) First, we obtain an approximate layout of curves  $T_{\text{eff}}(\lambda_1, D) = T_k = \text{const.}$ ; 2) The shape of the approximate curves  $T_k = \text{const.}$  is then corrected by iteration. In what follows, a detailed explanation of the procedure used is presented.

### 1) Approximate system of curves $T_{\text{eff}}(\lambda_1, D) = T_k = \text{const.}$ :

The system is established as the mean regression curve between the variables  $x$  and  $y$  from a set of measured pairs of points  $(x, y)$ . The regression  $x = x(y)$  does not necessarily represent the same locus of points as the one calculated in the form  $y = y(x)$ , nonetheless issued from the same  $(x, y)$  data set. The bisection curve between the direct  $x = x(y)$  and the inverse function  $x = y^{-1}(x)$  can then be used to represent the sought relation. Thus, in this work we calculate two series of functions to obtain the approximate average/bisection system of  $\lambda_1 = \lambda_1(D|T_k)$  curves<sup>1</sup>, where  $T_k = \text{const.}$  with  $k = 1, 2, \dots, N_K$  are constant values of the effective temperature:

i) A series of  $N_K$  regression polynomials  $\lambda_1 = \lambda_1(D)$  is calculated using stars whose effective temperatures are in intervals  $(T_k - \Delta T_k, T_k + \Delta T_k)$ , where  $\Delta T_k/T_k = 0.05$ . For a given  $T_k$  the obtained regression polynomial is assigned to the average  $\overline{T}_k$  temperature calculated from those entering the interval  $(T_k - \Delta T_k, T_k + \Delta T_k)$ ;

ii) With the  $T_{\text{eff}}^f$  values of stars lying in successive strips of constant  $\lambda_1$  parameters and total width  $\Delta\lambda_1 = 10 \text{ \AA}$  in the  $(\lambda_1, D)$  plane, we obtained a series of curves  $T_{\text{eff}}^f = T_{\text{eff}}^f(D|\langle\lambda_1\rangle)$ , where  $\langle\lambda_1\rangle$  is the average of  $\lambda_1$  parameters of the stars entering a given strip, as shown in Fig. 9a for two  $\langle\lambda_1\rangle$  values. Then, for a given  $\overline{T}_k$  temperature obtained in step i), we read the ab-

<sup>1</sup> Here, the notation  $F = F(u|v)$  means that  $F$  is a function of  $u$ , so that  $v = v(F, u) = \text{constant}$  over the entire space of variables  $(F, u)$ .

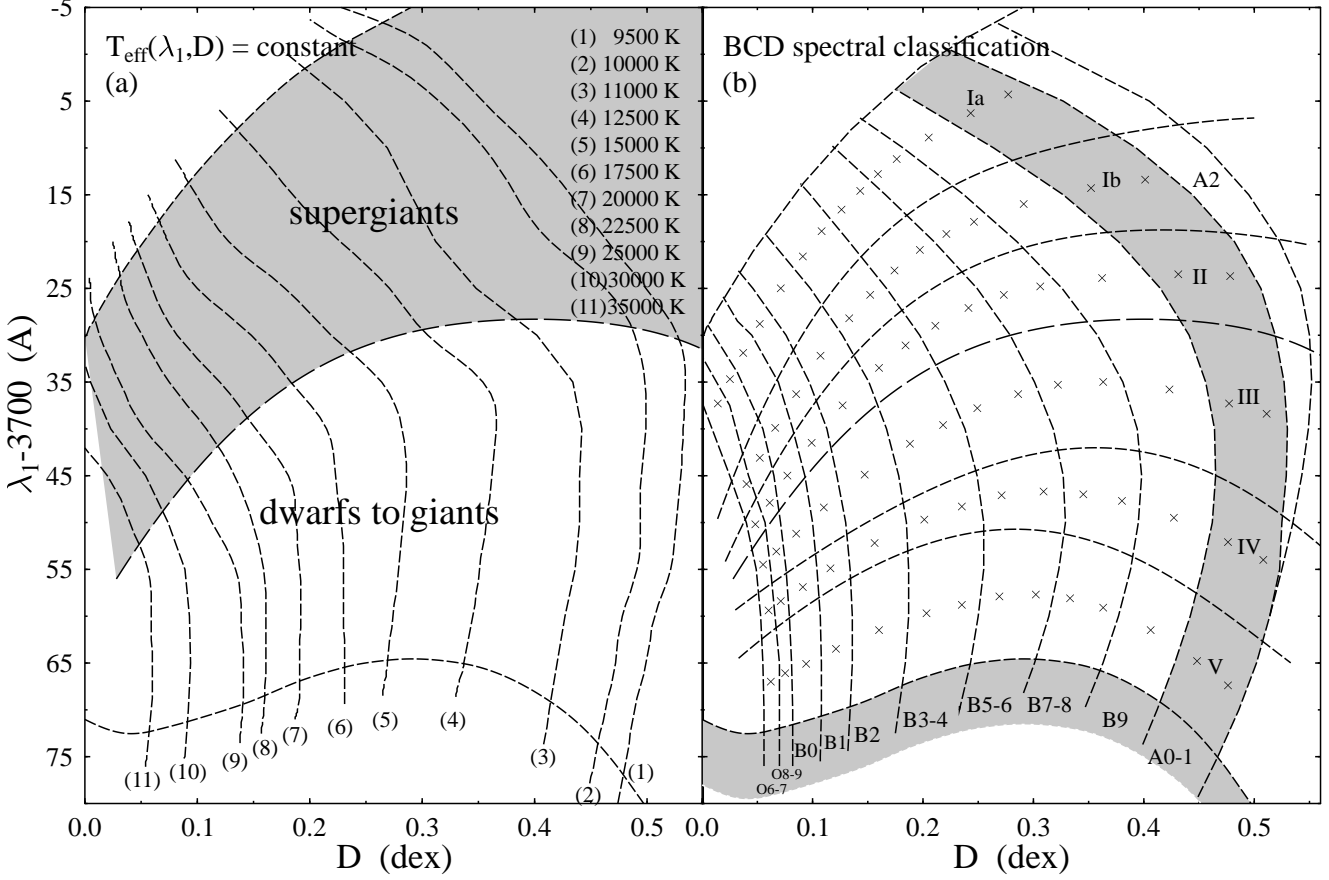


**Fig. 10.** (a): Spline-smoothed  $T_{\text{eff}}(\lambda_1, D) = \text{const}$  curves for the values of effective temperature given in the box at right-top; (b) The curvilinear-quadrilateral BCD  $(\lambda_1, D)$  spectral classification diagram, where the corresponding 2D MK spectral types (bottom shaded strip) and the luminosity classes (left shaded strip) are indicated. The cross-marks indicate the mid-point of each MK spectral type-luminosity class box where the  $T_{\text{eff}}(\lambda_1, D)$  values given in Table 3 were obtained.

scissae determined by all the  $\langle \lambda_1 \rangle = \langle \lambda_1 \rangle(D)$  curves, as in the example shown in Fig. 9a for the particular case  $\overline{T}_k = 15\,000$  K, to draw the corresponding  $\langle \lambda_1 \rangle = \langle \lambda_1 \rangle(D|\overline{T}_k)$  (see Fig. 9b, dashed curve).

The final curve adopted as the first approach to  $\overline{T}_k(\lambda_1, D) = \text{const.}$ , here called  $\widehat{\lambda}_1 = \widehat{\lambda}_1(D|\overline{T}_k)$ , is the smoothed bisecting locus of points (full line in Fig. 9b) between the regression polynomial  $\lambda_1 = \lambda_1(D|\overline{T}_k)$  obtained in *i*) (dotted line in Fig. 9b) and the homologous one  $\langle \lambda_1 \rangle = \langle \lambda_1 \rangle(D|\overline{T}_k)$  constructed in *ii*). Using a second order interpolation, the set of  $\widehat{\lambda}_1 = \widehat{\lambda}_1(D|\overline{T}_k)$  curves with  $k = 1, 2, \dots, N_K$  is then transformed into  $\widehat{\lambda}_1 = \widehat{\lambda}_1(D|T_k)$  curves, where  $T_k = 9\,500, 10\,000, \dots, 35\,000$  K are rounded integer values used in the following step. Hereafter the curves  $\widehat{\lambda}_1(D|\overline{T}_k)$  are called  $\lambda_1(D|T_k)$ .

## 2) Corrected $T_{\text{eff}}(\lambda_1, D) = \text{const}$ curves:

The layout of  $T_k(\lambda_1, D) = \text{const}$  curves obtained in 1) in principle might be adopted as the sought calibration. We have noticed, however, that we can reduce even more the residuals  $\epsilon_{T_{\text{eff}}} = |T_{\text{eff}}(\lambda_1^*, D^*) - T_{\text{eff}}^f|$ , where  $T_{\text{eff}}(\lambda_1^*, D^*)$  represents the temperature read in the calibrated  $(\lambda_1, D)$  plane for the star whose parameters are  $(\lambda_1^*, D^*, T_{\text{eff}}^f)$ . To reduce  $\epsilon_{T_{\text{eff}}}$  somewhat, we proceed as follows. We consider a star whose parameters are  $(\lambda_1^*, D^*, T_{\text{eff}}^f)$ . We call  $D_{k-1}, D_k, D_{k+1}$  and  $D_{k+2}$  the abscis-

sae of the intersections of the  $\lambda_1 = \lambda_1^*$  line with the curves of constant effective temperature  $\lambda_1 = \lambda_1(D|T_k)$ , ordered so that  $T_{k-1} > T_k > T_{\text{eff}}^f > T_{k+1} > T_{k+2}$ . We calculated the ‘corrected’ abscissae  $D'_k, D'_{k+1}$  of the curves  $T_k$  and  $T_{k+1}$  at  $\lambda_1 = \lambda_1^*$  with:

$$\begin{aligned} D'_k &= D^* + \left( \frac{1/T_k - 1/T_{\text{eff}}^f}{1/T_{k-1} - 1/T_{\text{eff}}^f} \right) (D_{k-1} - D^*) \\ D'_{k+1} &= D^* + \left( \frac{1/T_{k+1} - 1/T_{\text{eff}}^f}{1/T_{k+2} - 1/T_{\text{eff}}^f} \right) (D_{k+2} - D^*). \end{aligned} \quad (23)$$

For a given  $(\lambda_1^*, D^*)$ , the abscissae  $D_{k-1}$  and  $D_{k+2}$  are maintained unchanged (see Fig. 9c). This operation is done for all program stars, so that each of them contributes with its corresponding correcting displacement  $D' - D$ . In this way the position of each curve  $T_k = \text{const.}$  depends also on the nearest ones. The smoothed curve passing through the new  $(\lambda_1, D')$  points relative to the same  $T_k = \text{const.}$  is considered as the new  $\lambda_1 = \lambda_1(D|T_k)$  curve. Thus, at each iteration the whole system of  $T_k$  curves is somewhat modified. The iteration is continued until two conditions are obeyed: 1) the correlation of the read effective temperatures of the program stars in the newly obtained layout of  $T_{\text{eff}} = \text{const}$  curves as a function of the respective  $T_{\text{eff}}^f$  values does not show any systematic deviation

from the first diagonal; 2) the dispersion of points around this line attains its lowest possible value.

The  $T_{\text{eff}}(\lambda_1, D)$  diagram thus obtained is shown in Fig. 10a. The upper limiting curve in the diagram of Fig. 10a corresponds to the lowest  $\lambda_1$  parameters ever observed in the BCD system for OB supergiants. Whilst  $\lambda_1$  values higher than the bottom limiting curve of this diagram have never been measured for normal dwarf OB stars, they are normally observed for O sub-dwarfs and/or white dwarfs.

The method used to obtain the curves of constant  $T_{\text{eff}}(\lambda_1, D)$  makes the position of each  $T_{\text{eff}} = \text{const}$  curve depend on the global  $T_{\text{eff}}(\lambda_1, D)$  pattern; i.e. a change in one of these curves has an incidence on the shape of the surrounding curves. We also notice that the layout of the  $T_{\text{eff}} = \text{const}$  curves in the sector of supergiants is strongly constrained by the way the curves are arranged in the  $(\lambda_1, D)$  region of dwarfs and giants which are traced by a large sample of stars, and by the natural limiting condition which imposes that  $D \rightarrow 0$  as  $\lambda_1$  becomes negative. Actually, before the limit  $D \rightarrow 0$  is attained, for supergiants with  $T_{\text{eff}} \geq 25\,000$  K, there is a luminosity class interval, roughly from  $\lambda_1 - 3700 \sim 55 \text{ \AA}$  to  $\lambda_1 - 3700 \sim 5 \text{ \AA}$ , the extended low density atmosphere of these stars behaves like the circumstellar envelope of Be stars, producing  $D < 0$ , i.e. an emission-like Balmer discontinuity. The black body-like behavior  $D = 0$  is reached for the theoretical limit  $\lambda_1 - 3700 \sim -47 \text{ \AA}$ .

To examine the correspondence between the  $T_{\text{eff}}$  values and the MK spectral classes, we show in Fig. 10b the calibration of the BCD  $(\lambda_1, D)$  surface into B-spectral subtypes and luminosity classes. We can see that the pattern of  $T_{\text{eff}} = \text{const}$  curves mirrors the empirical MK spectral type calibration. The delimiting strips of constant sub-spectral types are determined with color gradient curves  $\Phi_{rb} = \text{const}$ . This system of curves resembles each other because the color temperature in the wavelength region over which  $\Phi_{rb}$  is defined is close to the stellar effective temperature. In Table 6 we give the values of  $T_{\text{eff}}$  for the points marked in Fig. 10b with crosses. These are mid-points of more or less large curvilinear boxes corresponding to a given MK SpT/LC. We note that it may not be straightforward to compare the effective temperatures for the nominal MK SpT/LCs given in Table 6 with the average values determined in the literature for the same MK spectral classes. This is because the baricenters of the  $(\lambda_1, D)$  parameters in these averages may not correspond to the mid-points of the curvilinear quadrilaterals given here (see crosses in Fig. 10b).

Finally, to verify the reliability of the new BCD  $T_{\text{eff}}$  calibration, in Fig. 11 we compare the effective temperatures of the program stars read in the  $(\lambda_1, D)$  calibration to those derived with bolometric fluxes. The comparison reveals a good correlation, where the dispersion of points around the first diagonal remains within a constant limit  $\Delta T_{\text{eff}}/T_{\text{eff}} = \pm 0.17$ . Considering that the  $T_{\text{eff}}^f$  values represent the reference for our  $T_{\text{eff}}(\lambda_1, D)$  calibration, the read  $T_{\text{eff}}$  values in the  $(\lambda_1, D)$  plane can be considered as affected by two kinds of uncertainties, one of them inherent to the measurement of the Balmer discontinuity, and the other related to the obtained layout of the  $T_{\text{eff}} = \text{constant}$  curves. Since the deviation of points around the first diagonal in Fig. 11 has a Gaussian distribution, which lies in the whole

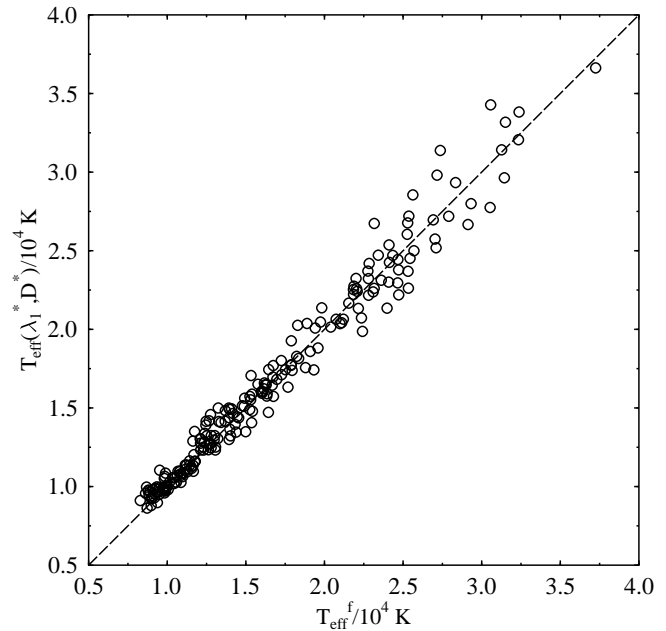


**Fig. 11.** Comparison between effective temperatures read in the  $(\lambda_1, D)$  plane (ordinates) and those derived with bolometric fluxes of the program stars (abscissa).

$3\sigma/T_{\text{eff}} = \pm 0.17$  interval, the expected total average error affecting the read  $T_{\text{eff}}(\lambda_1, D)$  quantities is thus (Smart 1958):

$$\frac{\bar{\epsilon}}{T_{\text{eff}}} = \sqrt{\frac{2}{\pi}} \frac{\sigma}{T_{\text{eff}}} \simeq \pm 0.05, \quad (24)$$

which is valid for the entire calibrated  $(\lambda_1, D)$  plane.

## 8. Discussion

In this work we have obtained a new  $T_{\text{eff}}(\lambda_1, D)$  calibration which is homogeneous over the entire BCD plane of  $(\lambda_1, D)$  parameters corresponding to early-type stars. For dwarfs and giants, this calibration yields  $T_{\text{eff}}$  values which are consistent with those derived using photometric and spectroscopic techniques, and with model atmospheres. However, for supergiants our  $T_{\text{eff}}$  estimates show rather high systematic discrepancies with the  $T_{\text{eff}}$  values derived by McErlean et al. (1999) with wind-free models of stellar atmospheres (see Fig. 7). As seen in Fig. 7, the wind-free model-dependent  $T_{\text{eff}}$  values are systematically higher than ours. Our  $T_{\text{eff}}$  estimates are also lower than those obtained with non-LTE BW models around  $T_{\text{eff}} \sim 25\,000$  K, but the discrepancies are smaller. From the discussion in §5.1, it appears that our  $T_{\text{eff}}^f$  estimates for supergiants could have possible systematic underestimates ranging from 500 K to about 700 K as the effective temperature goes from 20 000 K to 30 000 K. Although this can partially account for the deviation of points belonging to the  $T_{\text{eff}}^{(6)}$  group (crosses), it cannot explain the points above the the one-to-one line in Fig. 7 from other groups, because the systematic underestimations of our  $T_{\text{eff}}^f$  values are lower than 1 000 K. We suggest that the  $T_{\text{eff}}$  values determined through line profile fitting with synthetic spectra obtained with non-LTE BW model atmospheres, which in

**Table 6.** Effective temperatures at the mid-point of each curvilinear quadrilateral representing a MK spectral type-luminosity class in the BCD ( $\lambda_1, D$ ) plane for early type stars.

LC :	V			IV			III			II			Ib			Ia		
SpT	$\lambda_1$	$D$	$T_{\text{eff}}$															
O6-7	67.0	0.062	34640	59.4	0.060	34800	54.5	0.055	35060	50.2	0.048	33970	45.9	0.040	32590	37.3	0.014	29670
O8-9	66.1	0.075	32750	58.4	0.071	33070	53.1	0.067	32460	47.9	0.061	30690	43.1	0.052	28350	34.7	0.025	26040
B0	65.1	0.094	30000	56.9	0.091	29970	51.2	0.085	29070	45.0	0.077	26710	39.9	0.066	24380	31.9	0.037	23890
B1	63.5	0.121	27080	54.9	0.116	26960	48.4	0.110	24880	41.5	0.099	23370	36.3	0.085	22360	28.8	0.052	22020
B2	61.5	0.160	22620	52.2	0.156	22380	44.9	0.147	21740	37.5	0.127	20570	32.2	0.107	19790	25.0	0.071	19310
B3	59.7	0.203	19270	49.7	0.201	19160	41.6	0.188	18900	33.5	0.160	18010	28.2	0.133	17520	21.6	0.091	17140
B4	58.8	0.235	17220	48.3	0.235	17130	39.6	0.218	17310	31.1	0.184	16500	25.7	0.152	16180	18.9	0.108	15660
B5	57.9	0.269	15380	47.1	0.271	15570	37.8	0.249	15890	29.0	0.211	15080	23.1	0.174	14770	16.6	0.126	14460
B6	57.7	0.302	14100	46.7	0.309	14200	36.3	0.286	14530	27.1	0.241	13790	20.9	0.197	13510	14.6	0.143	13560
B7	58.1	0.333	13000	47.0	0.345	13000	35.3	0.322	13460	25.7	0.273	12600	19.2	0.221	12540	12.8	0.159	12800
B8	59.1	0.363	12190	47.7	0.380	12120	35.0	0.363	12380	24.8	0.306	11790	17.9	0.246	11930	11.2	0.176	12280
B9	61.5	0.406	11340	49.5	0.427	11240	35.8	0.423	11240	23.9	0.362	10800	16.0	0.291	11070	8.9	0.205	11720
A0	64.8	0.448	10470	52.1	0.476	10310	37.3	0.477	10350	23.5	0.431	10140	14.3	0.352	10310	6.3	0.243	11010
A1	67.4	0.476	9860	54.0	0.508	9730	38.4	0.511	9820	23.7	0.478	9680	13.4	0.401	9690	4.3	0.277	10440

LC = Luminosity class; SpT = spectral type

$[\lambda_1] = \lambda_1 - 3700 \text{ \AA}$ ;  $[D] = \text{dex}$

most cases are isothermal, could be partially responsible for the observed effective temperature discrepancies. It should not be neglected either that some discrepancies could arise due to problematic convergences of models in the diluted external atmospheric layers of supergiants (Crivellari & Simonneau 1991; Simonneau & Crivellari 1993; Crivellari & Simonneau 1994; Simonneau & Crivellari 1994).

### 8.1. Effects due to metallicity

The present BCD  $T_{\text{eff}}$  calibration was obtained using a sample of stars near the Sun, which are characterized by an average metallicity  $Z = 0.02$ . We might then expect systematic differences between our  $T_{\text{eff}}(\lambda_1, D)$  estimates and those for stars having lower metallicities, as in the Magellanic Clouds. Since stars of the same mass, but with lower  $Z$ , have smaller radii, we cannot ensure that a given  $T_{\text{eff}}^f$  can correspond to the same pair  $(\lambda_1, D)$  of a Magellanic Cloud-star. We can then wonder whether the  $T_{\text{eff}}^f$ -based calibration of the  $(\lambda_1, D)$  parameters obtained here can be used for stars with  $Z = 0.004$  and lower. To assess possible systematic differences in the  $T_{\text{eff}}$  estimates caused by the use of the present  $T_{\text{eff}}(\lambda_1, D)$  calibration for stars with an initial metallicity other than  $Z = 0.02$ , we calculated the BD using model atmospheres for  $Z = 0.002$ ,  $0.0002$ , and  $Z = 0.2$ , using the grids of ATLAS9 model atmospheres calculated by Castelli & Kurucz (2003). The results are displayed in Table 7. We have not extrapolated the fluxes to lower  $\log g$  values because of the difficulties of model convergence that cannot ensure reliable  $D$  values. In this table we see that for given values of  $\log g$  and  $T_{\text{eff}}$ , the  $D$  parameter is larger the lower the metallicity. Although the differences in the values of  $D$  depend on  $T_{\text{eff}}$  and  $\log g$ , on average we have  $D(Z=0.002) - D(Z=0.02) = 0.014 \pm 0.003$ ,  $D(Z=0.0002) - D(Z=0.02) = 0.023 \pm 0.005$ ;

$D(Z=0.2) - D(Z=0.02) = -0.019 \pm 0.008$ . These differences are slightly larger than those expected from the intrinsic uncertainties of the  $D$  values. The present BCD calibration of effective temperatures would then produce slightly underestimated  $T_{\text{eff}}$  values for  $(\lambda_1, D)$  pairs of stars in environments with  $Z < 0.02$ , or overestimated if  $Z > 0.02$ . In both cases the  $T_{\text{eff}}(\lambda_1, D)$  of stars in environments with  $Z \neq 0.02$  determined with the present calibration can be easily corrected using Table 7. The present  $T_{\text{eff}}^f$ -based calibration of the  $(\lambda_1, D)$  may be interesting also for early-type stars in the Magellanic Clouds, since there are no systematic measurements of far-UV fluxes that would enable us to use the BFM to obtain their  $T_{\text{eff}}^f$ .

In Fig. 12 we show the relation between the effective temperature and the Balmer discontinuity. Figure 12a refers to the relations issued from the calibration obtained in this work, where the values are for the mid-points of the spectral type-luminosity class curvilinear quadrilaterals in the BCD plane of  $(\lambda_1, D)$  parameters (c.f. Table 6). In this figure we indicate the lines of constant mean MK spectral type of stars in different average luminosity classes near the Sun. In Fig. 12b we show the  $(T_{\text{eff}}, D)$  curves calculated with wind-free models (Castelli & Kurucz 2003) for several  $\log g$  values and the standard metallicity  $Z = 0.02$ . The gray-shaded region corresponds to  $(T_{\text{eff}}, D)$  curves for  $Z = 0.0002$  and for the same set of  $\log g$  parameters as for  $Z = 0.02$ . For comparison sake, the hatched zone demarcates the region occupied by the empirical curves displayed in Fig. 12a. This shows that while wind-free model atmospheres can account reasonably for the  $(T_{\text{eff}}, D)$  relations from dwarfs to giants, they fail to do so for supergiants, and that the problem is particularly acute for supergiants with  $T_{\text{eff}} \gtrsim 20000$  K. It is expected that non-LTE BW models of hot supergiants can explain more easily the observed  $(T_{\text{eff}}, D)$  relations, since such atmospheres are heated by the backward wind

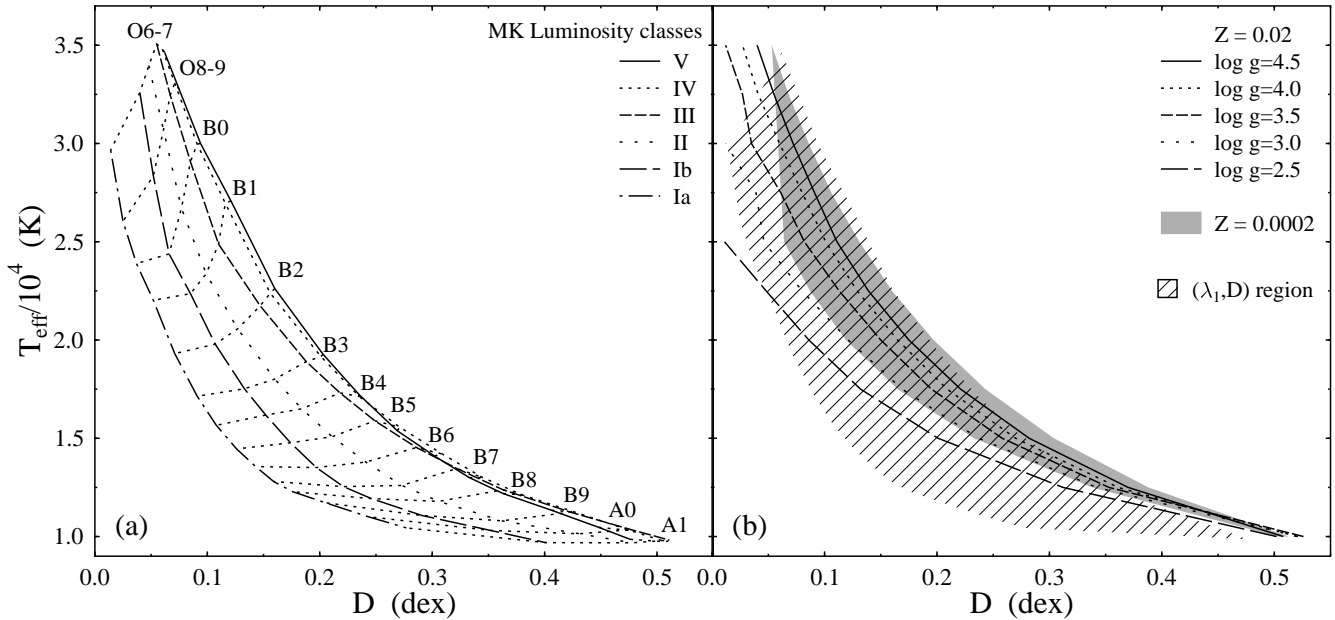


**Fig. 12.** (a): Effective temperature  $T_{\text{eff}}(\lambda_1, D)$  against the Balmer discontinuity for different average MK luminosity classes and spectral types. The letters OBA head the lines of constant spectral type; (b)  $T_{\text{eff}} = T_{\text{eff}}(D, \log g)$  relations from wind-free model atmospheres with metallicity  $Z = 0.02$ . The gray region corresponds to  $T_{\text{eff}} = T_{\text{eff}}(D, \log g)$  relations for metallicity  $Z = 0.0002$  and the same  $\log g$  parameters. The shaded zone corresponds to the empirical  $T_{\text{eff}}(\lambda_1, D)$  curves from panel (a) of this figure.

radiation, and the corresponding  $D$  values should then become smaller.

## 8.2. Effects related to the rotation

The new calibration of the  $(\lambda_1, D)$  plane as a function of  $T_{\text{eff}}$  was done assuming that all stars can be characterized by two parameters:  $T_{\text{eff}}$  and  $\log g$ . It was shown by Frémat et al. (2005) that also the apparent visual spectral region emitted by the non-uniform and geometrically deformed surface of fast rotating early type stars can be well represented with parent non-rotating  $T_{\text{eff}}$  and  $\log g$  parametric counterparts. The present calibration can then provide a first step for the interpretation of spectra emitted by rotating early-type objects, as already shown in Levenhagen et al. (2003); Neiner et al. (2003); Zorec et al. (2005); Vinicius et al. (2006); Frémat et al. (2006); Martayan et al. (2006, 2007); Floquet et al. (2000, 2002).

Rotation can also induce internal mixing of chemical elements. The mixing and transport of chemical elements throughout the star, produced in the stellar core, can be stronger with higher stellar rotation and it can be enhanced if the metallicity is low (Meynet & Maeder 2000, 2002). In particular, this may concern helium, whose abundance could then be larger in the atmospheres of evolved stars. Since this excess of He contributes to the absorption in the stellar surface layers, the value of the Balmer discontinuity can be affected. It was shown by Cidale et al. (2007) that in hot dwarf stars the larger the He abundance the smaller the value of  $D$ .

In order to see in more detail the influence of the He/H abundance ratio on the emitted visual energy distribution, a grid of synthetic spectra for a range of effective temperatures

was computed in non-LTE using the TLUSTY and SYNSPEC computing codes (Hubeny & Lanz 1995) and the references therein, assuming model atmospheres with He/H ratios of 0.1, 0.2, 0.5 and 1.0, and  $Z = 0.02$ . The atomic models we used are basically those provided on the TLUSTY website for H I (9 levels), He I (20 individual levels) and He II (20 levels). In all cases, the micro-turbulence velocity was supposed to be  $2 \text{ km s}^{-1}$ . We have reduced the synthetic spectra to the BCD resolution and calculated the BDs following the procedure used for the empirical ones. In Table 9 we give the obtained differences  $\delta D = D - D(0.1)$  as a function of the model ( $T_{\text{eff}}, \log g, \text{He/H}$ ) parameters. Here  $D(0.1)$  indicates that  $D$  is for the He/H = 0.1 abundance ratio. In this table we see that on average  $\delta D < 0$  and that  $|\delta D|$  is larger the higher the He/H abundance ratio and for  $19000 \leq T_{\text{eff}} \leq 23000 \text{ K}$ . In recent studies of supergiants Repolust et al. (2005); Crowther et al. (2006); Searle et al. (2008); Markova & Puls (2008) have found that an abundance He/H = 0.2 fits their atmospheres. From Table 9 we see that a ratio He/H = 0.2 effects the value of  $D$  by less than the error of measurement of  $D$ . Nevertheless, these differences are systematic and can be important for the hottest supergiants. In table (Table 8) we give the increments  $\delta T_{\text{eff}}$  that can be produced on the  $T_{\text{eff}}$  values for  $\log g = 3.0$  by  $\delta D(0.2) = D(\text{He/H}=0.2) - D(\text{He/H}=0.1)$  with respect to the  $T_{\text{eff}}(D)$  scale at He/H = 0.1 given in Table 7.

We note that: 1) Only those stars that were fast rotators during their Main Sequence evolutionary phase are likely to show an atmospheric increase of the He/H ratio in their blue supergiant phase; 2) The energy distributions in the near-IR where the angular diameter  $\theta^f$  is calculated, using models for He/H = 0.1 and He/H = 0.2, give the same flux levels. Moreover, in

**Table 7.** Balmer discontinuities  $D$  as a function of  $T_{\text{eff}}$  and  $\log g$  for different metallicities  $Z$ .

$T_{\text{eff}}$	$\log g$					
	4.5	4.0	3.5	3.0	2.5	2.0
$Z = 0.02$						
10000	0.508	0.520	0.526	0.521	0.502	0.452
12500	0.370	0.361	0.353	0.342	0.312	0.281
15000	0.282	0.270	0.258	0.237	0.201	0.168
17500	0.221	0.209	0.195	0.169	0.132	0.097
20000	0.175	0.165	0.150	0.121	0.086	
22500	0.139	0.129	0.113	0.080	0.048	
25000	0.111	0.101	0.082	0.052	0.011	
27500	0.091	0.080	0.061	0.030		
30000	0.072	0.060	0.035	0.012		
32500	0.055	0.041	0.027			
35000	0.040	0.027	0.012			
$Z = 0.002$						
10000	0.511	0.523	0.526	0.518	0.500	0.457
12500	0.380	0.376	0.368	0.357	0.326	0.295
15000	0.295	0.288	0.276	0.257	0.222	0.190
17500	0.234	0.227	0.213	0.188	0.155	0.122
20000	0.189	0.181	0.166	0.139	0.108	
22500	0.153	0.145	0.129	0.102	0.074	
25000	0.125	0.115	0.099	0.073	0.048	
27500	0.101	0.091	0.074	0.050		
30000	0.082	0.070	0.052	0.032		
32500	0.065	0.052	0.034			
35000	0.051	0.036	0.018			
$Z = 0.0002$						
10000	0.513	0.524	0.528	0.521	0.503	0.462
12500	0.388	0.385	0.379	0.366	0.338	0.308
15000	0.304	0.298	0.287	0.266	0.233	0.201
17500	0.243	0.236	0.223	0.199	0.165	0.133
20000	0.197	0.189	0.175	0.150	0.119	
22500	0.160	0.152	0.138	0.115	0.087	
25000	0.131	0.122	0.109	0.088	0.064	
27500	0.106	0.097	0.084	0.067		
30000	0.086	0.076	0.064	0.050		
32500	0.068	0.058	0.047			
35000	0.053	0.042	0.032			
$Z = 0.2$						
10000	0.499	0.515	0.528	0.525	0.507	0.458
12500	0.361	0.357	0.346	0.334	0.317	0.299
15000	0.265	0.258	0.248	0.222	0.200	0.181
17500	0.199	0.190	0.179	0.151	0.127	0.104
20000	0.151	0.142	0.127	0.103	0.079	
22500	0.115	0.106	0.089	0.070	0.048	
25000	0.088	0.079	0.061	0.046	0.027	
27500	0.067	0.058	0.041	0.028		
30000	0.050	0.040	0.027	0.014		
32500	0.037	0.026	0.017			
35000	0.024	0.014	0.011			

**Table 8.** Increments  $\delta T_{\text{eff}}$  carried by  $\delta D(0.2)$ .

$T_{\text{eff}}$ (K)						
17000	19000	21000	23000	25000	27000	30000
$\delta T_{\text{eff}}$ (K)						
+140	+170	+270	+590	+600	+610	+600

changes were obtained in the value of the bolometric correction  $\delta_{\text{UV}}$  between He/H = 0.1 and He/H = 0.2, so that the use of models for He/H = 0.2 in our BFM would not in principle change our  $T_{\text{eff}}^f$  estimates; 3) Even though the calculations of  $\delta D$  given in Table 9 concern wind-free model atmospheres, the low dependence of deviations  $\delta D$  with  $T_{\text{eff}}$  and  $\log g$  ensures that the inclusion of the non-LTE BW will not change the results noticeably.

**Table 9.** Differences of Balmer discontinuities  $\delta D = D(\text{He/H}) - D(0.1)$  at metallicity  $Z = 0.02$ , as a function of  $T_{\text{eff}}$ ,  $\log g$  and for different He/H abundance ratios.  $D(0.1)$  is for the He/H = 0.1 ratio.

$T_{\text{eff}}$	$\log g$	He/H=0.2	0.5	1.0
		$\delta D$ (dex)		
12500	3.0	+0.011	+0.007	+0.000
	3.5	-0.005	-0.006	-0.014
	4.0	-0.001	-0.004	-0.008
15000	3.0	+0.000	-0.014	-0.020
	3.5	-0.005	-0.014	-0.029
	4.0	-0.005	-0.014	-0.029
17000	3.0	-0.003	-0.019	-0.025
	3.5	-0.005	-0.016	-0.032
	4.0	-0.006	-0.016	-0.035
19000	3.0	-0.003	-0.020	-0.026
	3.5	-0.004	-0.016	-0.032
	4.0	-0.006	-0.017	-0.035
21000	3.0	-0.006	-0.019	-0.025
	3.5	-0.004	-0.014	-0.029
	4.0	-0.006	-0.016	-0.033
23000	3.0	-0.006	-0.017	-0.022
	3.5	-0.003	-0.013	-0.026
	4.0	-0.005	-0.015	-0.029
25000	3.0	-0.006	-0.014	-0.019
	3.5	-0.003	-0.011	-0.023
	4.0	-0.004	-0.013	-0.025
27000	3.0	-0.004	-0.010	-0.016
	3.5	-0.002	-0.009	-0.019
	4.0	-0.003	-0.011	-0.021
30000	3.0	-0.003	-0.005	-0.011
	3.5	-0.002	-0.007	-0.013
	4.0	-0.002	-0.008	-0.014

$\delta D = 0$  for all He/H abundance ratios at  $T_{\text{eff}} = 10000$  K

the very few cases with  $T_{\text{eff}} > 20000$  K where we have calculated the energy distributions in the far- and extreme-UV, no

## 9. Conclusions

In this work we have presented a new and homogeneous calibration of the BCD plane ( $\lambda_1, D$ ) as a function of  $T_{\text{eff}}$  for early-type stars of all luminosity classes, in particular supergiants, which complete a similar one made earlier only for dwarf to giant B-type stars (Divan & Zorec 1982). The present calibration is based on effective temperatures calculated with the bolometric-flux method for all program stars, whose individual uncertainties are on average  $\epsilon/T_{\text{eff}}^f = 0.05$ . The average error of the obtained  $T_{\text{eff}}$  values on the ( $\lambda_1, D$ ) plane is the same in all early spectral types and luminosity classes, and they are of the same order as for the individual  $T_{\text{eff}}^f$  values. The effective temperatures of OB supergiants derived in this work agree within some 2000 K with other determinations found in the literature, except with those issued from wind-free non-LTE plane-parallel models of stellar atmospheres, which produce overestimates of up to more than 5000 K near  $T_{\text{eff}} = 25000$  K.

The  $T_{\text{eff}}(\lambda_1, D)$  calibration has the advantage of using measurable parameters of the continuum spectrum around the Balmer discontinuity, which are strongly sensitive to the ionization balance of the photosphere and to its gas pressure. The BCD parameters ( $\lambda_1, D$ ) can be easily measured in spectra of low resolution and, even though  $D$  is slightly affected by the ISM extinction, the correction can be precisely and easily accounted for. This makes the ( $\lambda_1, D$ ) quantities useful for distant stars. Moreover, since their determination easily can be programmed for automatic measurements, they are convenient for studies of stars in clusters or other stellar systems observed with multi-object spectrographs and/or spectro-imaging devices. The BCD system can also be of interest in analyzing stars in far away galaxies that will be observed with the Extremely Large Telescopes in the near future. In this context, the present calibration of  $T_{\text{eff}}(\lambda_1, D)$ , together with those in preparation for  $\log g(\lambda_1, D)$  and  $M_{\text{bol}}(\lambda_1, D)$ , can be helpful in translating the data in terms of physical quantities such as  $T_{\text{eff}}$  and  $\log g$ . Furthermore, introducing small corrections, these calibrations can be applied to stars in environments with different initial metallicity.

The contamination of atmospheres in supergiants by He due to rotational mixing does reduce the value of the Balmer discontinuity. However, this change can exceed the average measurement uncertainty of this parameter only when the abundance ratio becomes  $\text{He}/\text{H} \gtrsim 0.05$ , which is twice as large as the value assumed today in the model atmospheres of supergiants. Nevertheless, differences of up to 600 K can be produced by the estimated values of  $T_{\text{eff}}$  if the  $D$  values affected by the abundance  $\text{He}/\text{H} \approx 0.2$  are used in  $T_{\text{eff}}(D)$  relations calculated for  $\text{He}/\text{H} \approx 0.1$  at temperatures ranging from 23 000 K to 30 000 K.

On average, due to the measurement errors of  $D$ , the obtained  $T_{\text{eff}}(\lambda_1, D)$  parameters are obtained within uncertainties that for all studied early spectral types and luminosity classes are of the order of  $\Delta T_{\text{eff}}/T_{\text{eff}} = 0.05$ , which is roughly the same as for the effective temperatures determined with the bolometric flux method. Since the temperatures obtained with the bolometric flux method are not strongly sensitive to the character-

istics of model atmospheres, they may be taken as a reference to study the properties of stellar atmospheres using theoretical spectroscopy.

The ( $\lambda_1, D$ ) parameters are less easily obtained for very hot stars. However, for active stars, like Be, B[e] and He-peculiar OB-types, the determination of BCD parameters might be as straightforward as it is for OB-type stars without emission. This is due to the fact that the photospheric component of BD is separated from that originating in the circumstellar environment.

*Acknowledgements.* We thank the referee whose careful reading, remarks and criticisms allowed a significant improvement in the presentation of our results. We thank Mrs Martine Usdin for the language editing of this paper. LC acknowledges financial support from the Agencia de Promoción Científica y Tecnológica (BID 1728 OC/AR PICT 111) and the Programa de Incentivos G11/089 of the National University of La Plata, Argentina.

## References

- Abbott, D. C. & Hummer, D. G. 1985, *ApJ*, 294, 286  
 Achmad, L., de Jager, C., & Nieuwenhuijzen, H. 1993, *A&AS*, 100, 465  
 Adelman, S. J., Pintado, O. I., Nieva, M. F., Rayle, K. E., & Sanders, Jr., S. E. 2002, *A&A*, 392, 1031  
 Allen, C. W. 1976, *Astrophysical Quantities* (*Astrophysical Quantities*, London: Athlone (3rd edition), 1976)  
 Baillet, A., Chalonge, D., & Divan, L. 1973, *Nouvelle Revue d'Optique*, 4, 151  
 Balona, L. A. 1984, *MNRAS*, 211, 973  
 Barbier, D. & Chalonge, D. 1941, *Annales d'Astrophysique*, 4, 30  
 Becker, S. R. & Butler, K. J. 1990, *A&A*, 235, 326  
 Beeckmans, F. & Hubert-Delplace, A. M. 1980, *A&A*, 86, 72  
 Benaglia, P., Vink, J. S., Martí, J., et al. 2007, *A&A*, 467, 1265  
 Blackwell, D. E. & Shallis, M. J. 1977, *MNRAS*, 180, 177  
 Boisse, P. 1990, *A&A*, 228, 483  
 Breger, M. 1976a, *ApJS*, 32, 1  
 Breger, M. 1976b, *ApJS*, 32, 7  
 Cardelli, J. A., Clayton, G. C., & Mathis, J. S. 1989, *ApJ*, 345, 245  
 Castelli, F. 1991, *A&A*, 251, 106  
 Castelli, F. & Kurucz, R. L. 2003, in *IAU Symposium*, Vol. 210, *Modelling of Stellar Atmospheres*, ed. N. Piskunov, W. W. Weiss, & D. F. Gray, 20P–+  
 Castelli, F. & Kurucz, R. L. 2006, *A&A*, 454, 333  
 Chalonge, D. & Divan, L. 1952, *AnAp*, 15, 201  
 Chalonge, D. & Divan, L. 1973, *A&A*, 23, 69  
 Chalonge, D. & Divan, L. 1973, *A&A*, 23, 69  
 Chalonge, D. & Divan, L. 1977, *A&A*, 55, 117  
 Chauville, J., Zorec, J., Ballereau, D., et al. 2001, *A&A*, 378, 861  
 Cidale, L. S., Arias, M. L., Torres, A. F., et al. 2007, *A&A*, 468, 263  
 Cidale, L. S., Zorec, J., & Tringaniello, L. 2001, *A&A*, 368, 160  
 Code, A. D., Bless, R. C., Davis, J., & Brown, R. H. 1976, *ApJ*, 203, 417  
 Crivellari, L. & Simonneau, E. 1991, *ApJ*, 367, 612

- Crivellari, L. & Simonneau, E. 1994, *ApJ*, 429, 331
- Crowther, P. A., Hillier, D. J., Evans, C. J., et al. 2002, *ApJ*, 579, 774
- Crowther, P. A., Lennon, D. J., & Walborn, N. R. 2006, *A&A*, 446, 279
- Cruzado, A., Zorec, J., Vázquez, A., & Ringuelet, A. 2007, *Boletín de la Asociación Argentina de Astronomía La Plata Argentina*, 50, 97
- Divan, L. 1992, in *Current Topics in Astrofundamental Physics*, ed. N. Sanchez & A. Zichichi, 685–700
- Divan, L. & Zorec, J. 1982, In *The Sci. Aspects of the Hipparcos Space Astrometry Mission*, ESA-SP, 177, 101
- Dufay, J. 1964, *Introduction to astrophysics: The stars* (IEEE Transactions on Applied Superconductivity)
- Floquet, M., Hubert, A. M., Hirata, R., et al. 2000, *A&A*, 362, 1020
- Floquet, M., Neiner, C., Janot-Pacheco, E., et al. 2002, *A&A*, 394, 137
- Frémat, Y., Neiner, C., Hubert, A.-M., et al. 2006, *A&A*, 451, 1053
- Frémat, Y., Zorec, J., Hubert, A. M., & Floquet, M. 2005, *A&A*, 440, 305
- Friedemann, C., Guertler, J., Schielicke, R., & Dorschner, J. 1983, *Astron. Nach.*, 304, 237
- Friedemann, C. & Roeder, U.-K. 1987, *Astron. Nach.*, 308, 41
- Gabler, R., Gabler, A., Kudritzki, R. P., Puls, J., & Pauldrach, A. 1989, *A&A*, 226, 162
- Guertler, J., Schielicke, R., Dorschner, J., & Friedemann, C. 1982, *Astron. Nach.*, 303, 705
- Gulati, R. K., Malagnini, M. L., & Morossi, C. 1987, *Journal of Astrophysics and Astronomy*, 8, 315
- Gulati, R. K., Malagnini, M. L., & Morossi, C. 1989, *A&AS*, 80, 73
- Hanbury Brown, R., Davis, J., & Allen, L. R. 1974, *MNRAS*, 167, 121
- Hartquist, T. W., Dyson, J. E., Pettini, M., & Smith, L. J. 1986, *MNRAS*, 221, 715
- Hauck, B. & Mermilliod, M. 1975, *A&AS*, 22, 235
- Hayes, D. S. & Latham, D. W. 1975, *ApJ*, 197, 593
- Herrero, A., Puls, J., & Najarro, F. 2002, *A&A*, 396, 949
- Hillier, D., Lanz, T., Heap, S. R., et al. 2003, *ApJ*, 588, 1039
- Hubeny, I. 1988, *Computer Physics Comm.*, 52, 103
- Hubeny, I. & Lanz, T. 1995, *ApJ*, 439, 875
- Jamar, C., Macau-Hercot, D., Monfils, A., et al. 1976, *ESA SR-27*
- Johnson, H. L. & Mitchell, R. I. 1975, *Rev. Mex. Astron. Astrofis.*, 1, 299
- Keenan, P. C. & Morgan, W. W. 1951, in *50th Anniversary of the Yerkes Observatory and Half a Century of Progress in Astrophysics*, ed. J. A. Hynek, 12–+
- Kudritzki, R. P., Bresolin, F., & Przybilla, N. 2003, *ApJ*, 582, 83
- Kudritzki, R. P., Puls, J., Lennon, D. J., et al. 1999, *A&A*, 350, 970
- Kurucz, R. L. 1979, *ApJS*, 40, 1
- Lamers, H. J. G. L. M., Snow, T. P., & Lindholm, D. M. 1995, *ApJ*, 455, 269
- Lang, K. R. 1992, *Astrophysical Data I. Planets and Stars*. (Astrophysical Data I. Planets and Stars, X, 937 pp. 33 figs.. Springer-Verlag Berlin Heidelberg New York)
- Lefever, K., Puls, J., & Aerts, C. 2007, *A&A*, 463, 1093
- Levenhagen, R. S., Leister, N. V., Zorec, J., et al. 2003, *A&A*, 400, 599
- Macau-Hercot, D., Jamar, C., Monfils, A., et al. 1978, *ESA SR-28*
- Malagnini, M. L., Faraggiana, R., & Morossi, C. 1983, *A&A*, 128, 375
- Malagnini, M. L., Morossi, C., Rossi, L., & Kurucz, R. L. 1986, *A&A*, 162, 140
- Malagnini, M. L. & Morossi, C. J. 1990, *A&AS*, 85, 1015
- Markova, N. & Puls, J. 2008, *A&A*, 478, 823
- Martayan, C., Frémat, Y., Hubert, A.-M., et al. 2006, *A&A*, 452, 273
- Martayan, C., Frémat, Y., Hubert, A.-M., et al. 2007, *A&A*, 462, 683
- Martins, F., Schaerer, D., & Hillier, D. J. 2005, *A&A*, 436, 1049
- McErlean, N. D., Lennon, D. J., & Dufton, P. L. 1999, *A&A*, 349, 553
- Meynet, G. & Maeder, A. 2000, *A&A*, 361, 101
- Meynet, G. & Maeder, A. 2002, *A&A*, 390, 561
- Moon, T. T. & Dworetzky, M. M. 1985, *MNRAS*, 217, 305
- Morisset, C., Schaerer, D., Bouret, J.-C., & Martins, F. 2004, *A&A*, 415, 577
- Morossi, C. & Crivellari, L. 1980, *A&A*, 41, 299
- Morossi, C. & Malagnini, M. L. 1985, *A&AS*, 60, 365
- Moujtahid, A. 1993, *Master Deg. Rep. Univ. Paris VII*
- Moujtahid, A., Zorec, J., Hubert, A. M., Garcia, A., & Burki, G. 1998, *A&AS*, 129, 289
- Napiwotzki, R., Schoenberner, D., & Wenske, V. 1993, *A&A*, 268, 653
- Neiner, C., Hubert, A.-M., Frémat, Y., et al. 2003, *A&A*, 409, 275
- O'Donnell, J. E. 1993, *ApJ*, 422, 158
- Pasinetti Fracassini, L. E., Pastori, L., Covino, S., & Pozzi, A. 2001, *A&A*, 367, 521
- Puls, J., Urbaneja, M. A., Venero, R., et al. 2005, *A&A*, 435, 669
- Remie, H. & Lamers, H. J. G. L. M. 1981, *A&A*, 105, 85
- Repolust, T., Puls, J., Hanson, M. M., Kudritzki, R.-P., & Mokiem, M. R. 2005, *A&A*, 440, 261
- Repolust, T., Puls, J., & Herrero, A. 2004, *A&A*, 415, 349
- Rohrman, R., Zorec, J., Cidale, L., Morrell, N., & Frémat, Y. 2003, in *Modelling of Stellar Atmospheres*, IAU Symposium 210, Eds N. Piskunov, W.W. Weiss, and D.F. Gray, ASP Conf. Ser., p. 26
- Searle, S. C., Prinja, R. K., Massa, D., & Ryans, R. A. 2008, *A&A*, 481, 777
- Simonneau, E. & Crivellari, L. 1994, *ApJ*, 428, 753
- Simonneau, E. & Crivellari, L. 1993, *ApJ*, 409, 830
- Smart, W. M. 1958, *Combination of observations* (Cambridge at the University Press)
- Smith, L. J., Norris, R. P. F., & Crowther, P. A. 2002, *MNRAS*, 337, 1309

- Springmann, U. W. E. & Pauldrach, A. W. A. 1992, A&A, 262, 515
- Trundle, C., Lennon, D. J., Puls, J., & Dufton, P. L. 2004, A&A, 417, 217
- Tüg, H. 1980, A&AS, 39, 67
- Underhill, A., Divan, L., Prevot-Burnichon, M.-L., & Doazan, V. 1979, MNRAS, 189, 601
- Underhill, A. & Doazan, V. 1982, in B-Stars with and Without Emission Lines, NASA-SP, 456, 60
- Underhill, A. B., ed. 1966, Astrophysics and Space Science Library, Vol. 6, The early type stars
- Vinicius, M. M. F., Zorec, J., Leister, N. V., & Levenhagen, R. S. 2006, A&A, 446, 643
- Vink, J. S., de Koter, A., & Lamers, H. J. G. L. M. 1999, A&A, 350, 181
- Wesselius, P. R., van Duinen, R. J., de Jonge, A. R. W., et al. 1982, A&AS, 49, 427
- Zorec, J. 1986, Thèse d'État, Université de Paris, VII
- Zorec, J. & Briot, D. 1985, RMAA, 10, 209
- Zorec, J. & Briot, D. 1991, A&A, 245, 150
- Zorec, J., Frémat, Y., & Cidale, L. 2005, A&A, 441, 235
- Zorec, J. & Mercado-Ibanez, R. 1987, in Academie des Sciences (Paris), Comptes Rendus, Serie II - Mecanique, Physique, Chimie, Sciences de l'Univers, Sciences de la Terre, Vol. 305, 1279

## Appendix A: About the BCD system

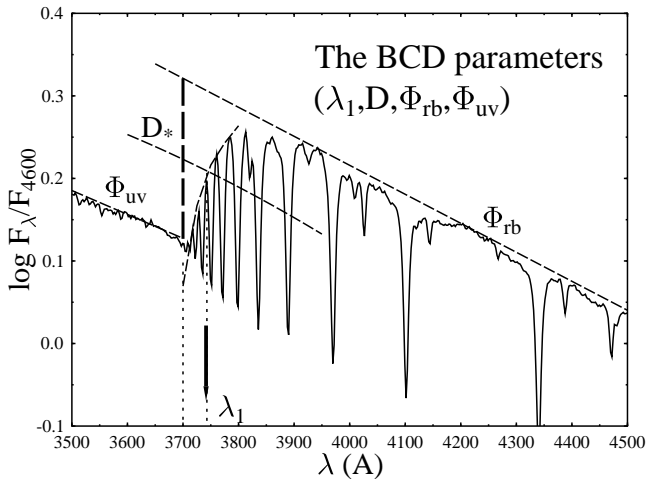


**Fig. A.1.** Graphical explanation of the BCD ( $\lambda_1$ ,  $D$ ,  $\Phi_{rb}$ ,  $\Phi_{uv}$ ) parameters.

Initially, the BCD (Barbier-Chalonge-Divan) system has been thought as a two-parameter system of stellar classification, based on the spectrophotometric study of the continuum spectrum around the Balmer discontinuity. It is used for O, B, A and F-type stars. The two parameters are the size of the Balmer jump,  $D$  given in dex, and its mean spectral position,  $\lambda_1$  given as the difference  $\lambda_1 - 3700$  in Å.

The value of  $D$  is calculated at  $\lambda = 3700$  Å, as  $D = \log_{10} F_{3700+} / F_{3700-}$ , where  $F_{3700+}$  is the Paschen side of the flux

and  $F_{3700-}$  is the flux in the Balmer continuum. The value of  $F_{3700+}$  is obtained by extrapolating the rectified Paschen continuum to  $\lambda = 3700$ , for which a relation such as  $\log F_\lambda / B_\lambda = p \times (1/\lambda) + q$  is used.  $B_\lambda$  can be the flux of a comparison star or simply the Planck function of a higher effective temperature than that expected for the studied star. In the present work we adopt the Planck function, so that the expression for  $D$  is:

$$D = \log \left[ \frac{F_{3700+} / B_{3700}}{F_{3700-} / B_{3700}} \right] \text{ dex} . \quad (\text{A.1})$$

For the empirical determination of  $D$ , spectra of low resolution are used:  $\Delta\lambda = 8$  Å at  $\lambda = 3700$ .

The average spectral position of the Balmer discontinuity is given by the point of intersection between the curve that passes over the maxima of fluxes in the limit of the Balmer line series, and the flux curve determined by the points  $\log F_\lambda - D/2$  on the Paschen side and  $\log F_\lambda + D/2$  on the Balmer side. In Fig. A.1 we show the method of determining  $D$  and  $\lambda_1$ . Since the wavelength scale to determine the intersection of flux curves is based on the intrinsic wavelengths of the identified spectral lines, the parameter  $\lambda_1$  is not affected by any displacements due to the radial velocity of stars.

When carrying out the spectrophotometric study of the energy distribution near the Balmer discontinuity, two other parameters are obtained: the color gradient  $\Phi_{uv}$ , given in  $\mu\text{m}$  and defined for the 3200–3700 Å spectral region, and the Paschen gradient defined in two versions:  $\Phi_b$  or  $\Phi_{rb}$  for the spectral regions 4000–4800 Å and 4000–6700 Å, respectively, both given in  $\mu\text{m}$ . A color gradient is defined as (Allen 1976):

$$\Phi = 5\lambda - \frac{d \ln F_\lambda}{d(1/\lambda)} , \quad (\text{A.2})$$

which for a black body at temperature  $T$ , becomes :

$$\Phi(T) = (C_2/T) (1 - e^{-C_2/\lambda T}) , \quad (\text{A.3})$$

where  $C_2 = hc/k = 1.4388$  cm deg is the radiation constant. Assuming that for a given stellar energy distribution  $F_\lambda$  it is  $\Phi = \text{const.}$  between wavelengths  $\lambda_a$  and  $\lambda_b$ , the expression for  $\Phi$  is:

$$\Phi = \ln \left[ \frac{\lambda_a^5 F_{\lambda_a}}{\lambda_b^5 F_{\lambda_b}} \right] / (1/\lambda_a - 1/\lambda_b) . \quad (\text{A.4})$$

The color gradient  $\Phi_b$  was introduced in 1955 in the BCD system to distinguish F-type stars from B-type stars having the same ( $\lambda_1$ ,  $D$ ) pairs. This parameter also has been used as a third BCD quantity related to the metal abundance of late type stars, in particular to the abundance ratio [Fe/H] (Chalonge & Divan 1977).

As the local temperature of the formation region of the Paschen continuum is close to the effective temperature, from (A.4) and (A.3) we note that stars with the same effective temperature but different surface gravity define a common region in the plane ( $\lambda_1$ ,  $D$ ). This fact was used by Barbier & Chalonge (1941) and Chalonge & Divan (1952) to determine the curvilinear quadrilaterals that characterize the BCD classification system. To this end, the authors used the MK classification of

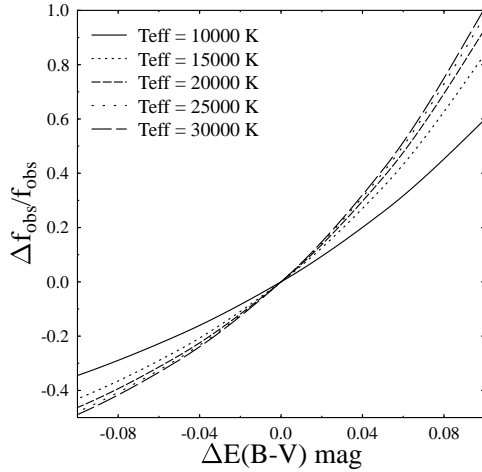


**Fig. B.1.** Error committed on the estimate of the observed fraction of the bolometric flux as a function of the uncertainty on the ISM color excess  $E(B - V)$ .

stars made by Morgan and Keenan (Keenan & Morgan 1951) themselves. They simply delimited the common region occupied by stars of the same MK spectral type with curves of intrinsic constant  $\Phi_{\text{tb}}$  parameters. The same technique was used to draw the ‘horizontal’ lines that separate the MK luminosity classes. The BCD authors attempted to keep inside a common strip stars of all spectral types, but having the same MK luminosity class label assigned by Morgan and Keenan.

The color gradients  $\Phi_b$  and  $\Phi_{\text{tb}}$  can be written as a function of the  $(B - V)$  color of the UBV photometric system (Moujtahid et al. 1998). The relation between the color excesses in the BCD and UBV systems due to the ISM reddening is then (Chalonge & Divan 1973):

$$A_V = 3.1E(B - V) = 1.7(\Phi_{\text{tb}} - \Phi_{\text{tb}}^o) = 1.9(\Phi_b - \Phi_b^o) \text{ mag}, \quad (\text{A.5})$$

where  $\Phi_{\text{tb}}^o$  is the stellar intrinsic color gradient.

*One of the greatest advantages of the BCD method is that low resolution spectra are used. Since the BCD parameters can be easily obtained through automatic treatment of data, they are convenient for studies of stars in clusters or other stellar systems observed with multi-object spectrographs and/or spectro-imaging devices. The BCD system can also be of interest to analyze stars in far away galaxies that will be observed with the Extremely Large Telescopes.*

## Appendix B: Calculation of the random errors affecting $T_{\text{eff}}^f$ and $\theta^f$

As quoted in §5.2, the  $T_{\text{eff}}^f$  and  $\theta^f$  parameters derived in the present work have the following sources of error: a) the ISM color excess  $E(B - V)$ ; b) the line blocking enhancement parameter  $\gamma$ ; c) the  $\log g$  parameter on which the model fluxes used to estimate the angular diameter depend and the filling factor due to the unobserved spectral region; d) the filling factor  $\delta$  used in relation (3) to calculate the bolometric flux.

a) *The ISM color excess  $E(B - V)$ .* The correction of the observed energy distributions for the ISM extinction is probably

the source of error that has the heaviest consequences on the determination of  $T_{\text{eff}}^f$ . Both the value of the bolometric flux  $f$  in Eq. (3) and the flux ratio  $f_{\lambda}^o/F_{\lambda}$  entering Eq. (2) depend on this correction.

We write the error on the estimate of the color excess  $E(B - V)$  as  $\Delta E = E(B - V) - E_o(B - V)$ , where  $E_o(B - V)$  is the ‘unknown’ correct value of this excess. The effect of  $\Delta E$  on the integrated fluxes coming from the observed spectral region,  $f_{\text{obs}}$ , can be estimated with model atmospheres, by calculating the ratio  $\Delta f_{\text{obs}}/f_{\text{obs}} = [f_{\text{obs}}(\Delta E) - f_{\text{obs}}]/f_{\text{obs}}$ . The behavior of  $\Delta f_{\text{obs}}/f_{\text{obs}}$  against  $\Delta E$  for several effective temperatures is shown in Fig. B.1. This calculation is made only for  $\log g = 3.0$  since the effect of  $\log g$  on  $\Delta f_{\text{obs}}/f_{\text{obs}}$  is negligible.

The uncertainty  $\Delta E$  also affects the monochromatic fluxes  $f_{\lambda}^o$  used to derive the angular diameter. The angular diameter affects  $T_{\text{eff}}^f$ , which, in turn, determines  $T_{\text{eff}}(\gamma)$  and the model flux entering relation (2). For an estimate of the ratio  $\Delta \theta^f/\theta^f$  we can simply use  $\lambda = 0.7 \mu\text{m}$ , the middle wavelength of the interval over which  $\theta^f$  is calculated. To make these calculations easier, the flux  $F_{\lambda 0.7}$  is represented as a function of  $T_{\text{eff}}(\gamma)$  and  $\log g$ , using the following interpolation expression:

$$\begin{aligned} F_{\lambda 0.7}[T_{\text{eff}}(\gamma), g] &= A(\log g)T_{\text{eff}}(\gamma)^{B(\log g)} \\ A(\log g) &= 5.383 - 2.351 \log g + 0.32073 \log^2 g \quad (\text{B.1}) \\ B(\log g) &= 1.405 + 0.191 \log g - 0.027 \log^2 g. \end{aligned}$$

For the observed stellar flux at  $\lambda = 0.7 \mu\text{m}$  corrected for the ISM extinction is  $f_{0.7}^o = f_{0.7}^{\text{obs}} 10^{0.4k_{0.7}E(B - V)}$ , with  $k_{0.7} = 2.39$ , using (B.1) the total uncertainty affecting the angular diameter can be written to the first order as:

$$\frac{\Delta \theta^f}{\theta^f} = 1.1\Delta E(B - V) - \frac{1}{2} \left\{ B(\log g) \frac{\Delta T_{\text{eff}}(\gamma)}{T_{\text{eff}}(\gamma)} + \left[ \frac{\partial \ln A(\log g)}{\partial \log g} + \ln T_{\text{eff}}(\gamma) \frac{\partial B(\log g)}{\partial \log g} \right] \Delta \log g \right\}, \quad (\text{B.2})$$

where it also includes the dependence on  $\Delta \log g$  and the uncertainty  $\delta \gamma$  in the factor  $\Delta T_{\text{eff}}(\gamma)/T_{\text{eff}}(\gamma)$ , whose dependence on  $\delta \gamma$  we shall discuss below.

In this work, the uncertainty inherent to  $E(B - V)$  was characterized with the  $1\sigma$  dispersion of the independent estimates of  $E(B - V)$  for a given star, i.e.  $\Delta E(B - V) = \pm \sigma_{E(B - V)}$ . For the studied stars, it is on average  $\sigma_{E(B - V)} \simeq 0.03$  mag. In (B.2) the direct dependence of  $\Delta \theta^f$  on  $\Delta E(B - V)$  is noted. However, it can be shown that the change of  $f_{0.7}^o$  with  $\Delta E(B - V)$  is larger than that of  $F_{0.7}$  induced by the corresponding  $\Delta T_{\text{eff}}^f$ . This means that if  $\Delta E(B - V)$  carries an increase of  $f_{0.7}^o$  and an overestimation of  $T_{\text{eff}}^f$  through a greater bolometric flux, the corresponding increase of  $F_{0.7}$  will compensate for the increase of  $f_{0.7}^o$ , which maintains  $\theta^f$  almost unchanged.

b) *The line blocking enhancement parameter  $\gamma$ .* To some degree, the estimate of  $\gamma$  is also dependent on the ISM extinction, whose effects in the far-UV can be confused with those produced by the line blanketing. The effect of the error on the enhancing factor  $\gamma$  can be important as it enters the determination of the temperature  $T_{\text{eff}}(\gamma)$  used to calculate both  $\theta$  and  $\delta$ . Nevertheless, the total effect of  $\gamma$  on the value of  $T_{\text{eff}}^f$  does not seem to carry larger deviations than  $\Delta T_{\text{eff}} \sim 300$  K, as shown in Fig. 2.

The relative error  $\Delta T_{\text{eff}}(\gamma)/T_{\text{eff}}(\gamma)$  as a function of the uncertainty on  $\gamma$  can be estimated using the relation (12). Since an interpolation expression of the function  $\Lambda$  as a function of  $T_{\text{eff}}(\gamma)$  and  $\log g$  is not easy to derive, to a good first order we can attempt an estimate of the uncertainty on  $T_{\text{eff}}(\gamma)$  produced by  $\Delta\gamma$ , with:

$$\frac{\Delta T_{\text{eff}}(\gamma)}{T_{\text{eff}}(\gamma)} \simeq \frac{1}{4} \Lambda[T_{\text{eff}}(\gamma), \log g] \Delta\gamma. \quad (\text{B.3})$$

The model fitting to the observed energy distributions carries uncertainties on the  $\gamma$  of the order of  $\Delta\gamma \simeq 0.25$ . The consequences of this uncertainty on the value of  $T_{\text{eff}}(\gamma)$  for a given  $T_{\text{eff}}^f$  can be derived using (B.3) or by interpolation in Table 1.

c) *The log g parameter.* We assumed that the adopted model energy distributions correspond to gravities determined within an error  $\Delta \log g = 0.5$  dex, which is twice the typical dispersion seen in Fig. 4.

d) *The filling factor  $\delta$ .* The bolometric flux fraction  $\delta$  would be realistic, if the actual stellar atmosphere of the observed star obeyed the basic assumptions that rule the models used. Although the non-LTE BW models produce somewhat different energy distributions in the far- and extreme-UV spectral regions, they cannot carry any significant change to the estimate of  $\delta$ , as compared to the values derived with wind-free models. Having no definite knowledge of the phenomena that models might still be missing, we assumed that we could have uncertainties affecting  $\delta$  of the order of  $\Delta\delta/\delta = 0.10$ .

Since the uncertainties mentioned in this section do not propagate symmetrically (i.e. see Table 4), their combined effect was simulated as follows. Let us call  $|\Delta_P|$  the absolute error assigned to a given  $P$  quantity, i.e.  $P = E(B - V)$ ,  $\gamma$ ,  $\log g$  and  $\delta$ . We divide each  $|\Delta_P|$  into 4 parts:  $\epsilon_P = |\Delta_P|/4$ , so that we can assign to each quantity  $P$  9 independent estimates, i.e.  $P \equiv P - 4\epsilon_P, P - 3\epsilon_P, \dots, P, \dots, P + 3\epsilon_P, P + 4\epsilon_P$ . Then, as we have 4 different parameters to which we assign an error, each of them is taken with one possible simulated value  $P \pm n\epsilon_P$  ( $n$  from 1 to 4); we have  $9^4 = 6561$  possible combinations that produce as many estimates of  $T_{\text{eff}}^f$  and  $\theta^f$  around the ‘central’ one where all  $\Delta_P = 0.0$ . The frequency of  $T_{\text{eff}}^f$  and  $\theta^f$  values thus obtained have a bell-shaped distribution, not always symmetric. Let us call  $Q(\epsilon_{T_{\text{eff}}})$  and  $Q(\epsilon_\theta)$  these distributions, where  $\epsilon_{T_{\text{eff}}} = T_{\text{eff}} - T_{\text{eff}}^o$  and  $\epsilon_\theta = \theta - \theta^o$  are the displacements from the respective  $T_{\text{eff}}^o$  and  $\theta^o$  values for which all  $\Delta_P = 0.0$ . The errors indicated in Table 2 are then the mean errors defined as:

$$\bar{\epsilon} = \int_{-\infty}^{+\infty} |\epsilon| Q(\epsilon) d\epsilon / \int_{-\infty}^{+\infty} Q(\epsilon) d\epsilon \quad (\text{B.4})$$

that would correspond to  $\bar{\epsilon} = \sqrt{2/\pi}\sigma$  if the distributions  $Q(\epsilon)$  are ‘normal’, Gaussian, with dispersion  $\sigma$ . On average it is  $\langle \bar{\epsilon}/T_{\text{eff}}^f \rangle \simeq 0.05$ , which is of the same order as the error expected for the  $T_{\text{eff}}(\lambda_1, D)$  values estimated in §7.2, c.f. relation (24).

Table 2: Program stars, observed and derived parameters.

HD	SpT/LC	$\lambda_1$	$D$ dex	$E(B - V)$ mag	$T_{\text{eff}}^f \pm \Delta T_{\text{eff}}$ K	$\theta^f \pm \Delta\theta$ mas	$\gamma$	$T_{\text{eff}}(\lambda_1, D)$ K
358	B5.5V	58.0	0.288	0.023	12750±590	1.016±0.010	1.00	14580
886	B2IV	54.0	0.155	0.007	21870±1390	0.444±0.021	1.00	22740
2905	B1Ia	31.0	0.070	0.339	22160±1420	0.348±0.021	1.13	21330
3360	B2IV	54.0	0.161	0.031	21850±1390	0.307±0.021	1.00	22220
3369	B5V	54.0	0.259	0.046	15980±910	0.305±0.015	1.00	16030
4142	B5.5V	59.0	0.283	0.044	16430±940	0.162±0.015	1.00	14720
4727	B4V	58.0	0.249	0.029	16290±930	0.266±0.015	1.00	16460
11241	B2V	65.0	0.162	0.066	22080±1410	0.141±0.021	1.00	22420
12767	B5V	55.1	0.279	0.000	13250±640	0.281±0.011	1.00	15000
12953	A2Ia	-1.0	0.231	0.599	9750±330	0.591±0.007	1.58	9940
13267	B6Ia	16.0	0.155	0.490	14380±760	0.259±0.012	0.76	13460
14055	A1V	71.0	0.471	0.019	9440±310	0.540±0.007	1.00	9840
14228	B6V	61.7	0.296	0.015	12470±560	0.507±0.010	1.00	14150
14489	A0Ib	11.0	0.310	0.420	9840±340	0.549±0.007	2.04	10650
14818	B2Ib-Ia	31.0	0.086	0.496	18300±1100	0.202±0.018	1.32	20260
15130	A0.5IV	52.8	0.490	0.019	9920±350	0.346±0.008	1.00	10040
15318	B9.5V	61.9	0.440	0.020	10630±400	0.421±0.008	1.00	10700
16046	A0IV	56.4	0.448	0.021	10910±420	0.314±0.008	1.00	10730
16582	B2IV	52.6	0.154	0.020	23160±1500	0.239±0.022	1.00	22610
16908	B4V	54.0	0.231	0.046	17520±1030	0.243±0.017	1.00	17430
17081	B6IV	46.0	0.311	0.016	13680±680	0.344±0.011	1.00	14150
17573	B7V	54.0	0.339	0.014	12980±610	0.476±0.010	1.00	12950
18604	B6V-IV	50.4	0.301	0.033	13940±710	0.286±0.011	1.00	14380
19356	B7V	60.0	0.324	0.047	12800±590	1.033±0.010	1.00	13240
20041	A0Ia	10.0	0.276	0.816	10800±420	0.643±0.008	2.02	10980
21291	B9Ia	9.0	0.213	0.495	11420±470	0.794±0.009	1.28	11640
21364	B7.5V	64.8	0.337	0.044	13070±620	0.473±0.010	1.00	12510
21389	A0Ia	4.0	0.233	0.633	11040±440	0.886±0.009	1.22	10860
21447	A1V	72.0	0.466	0.026	9240±300	0.337±0.007	1.00	9890
21790	B9IV	45.8	0.408	0.017	11760±500	0.317±0.009	1.00	11610
21856	B1IV	57.0	0.116	0.183	25370±1670	0.124±0.023	1.00	27200
22928	B5III	42.0	0.281	0.044	14890±820	0.583±0.013	1.00	15100
22951	B1V	62.0	0.112	0.253	29330±1980	0.183±0.024	1.00	27990
23180	B1III	49.0	0.121	0.267	22840±1470	0.384±0.021	0.97	24190
23227	B4.5III	43.4	0.247	0.019	16230±930	0.215±0.015	1.00	16470
23288	B7V	56.0	0.329	0.117	14020±720	0.224±0.011	1.00	13220
23324	B7V	56.0	0.334	0.061	13210±640	0.201±0.010	1.00	13050
23338	B6IV	46.0	0.296	0.059	14180±740	0.351±0.011	1.00	14650
23408	B6.5III	38.5	0.313	0.129	14310±750	0.464±0.011	1.00	13960
23625	B2V	59.0	0.175	0.294	23980±1560	0.114±0.022	1.00	21350
23753	B7IV	50.0	0.350	0.065	12680±580	0.228±0.010	1.00	12740
23850	B7III	39.0	0.339	0.086	13020±620	0.526±0.010	1.00	13240
23923	B9V	58.0	0.411	0.054	11640±490	0.170±0.009	1.00	11350
24131	B1V	61.0	0.124	0.265	29130±1960	0.132±0.024	1.00	26670
24398	B1Ib	37.0	0.085	0.328	22040±1410	0.659±0.021	0.98	22580
24431	O9.5III	54.0	0.077	0.653	27370±1830	0.155±0.023	1.41	31380
24760	B0IV-III	54.5	0.089	0.086	27160±1810	0.394±0.023	1.00	29810
25204	B4IV	50.1	0.243	0.050	16970±990	0.447±0.016	1.00	16829
25490	>A1V	74.0	0.496	0.007	8990±280	0.605±0.007	1.00	9300
27376	B6V	61.5	0.303	0.012	12460±560	0.522±0.010	1.00	13910
27396	B4IV	51.0	0.240	0.146	16720±970	0.267±0.016	1.00	16960
27962	A1V	71.0	0.463	0.000	8680±260	0.515±0.008	1.00	9970

Table 2: continued.

HD	SpT/LC	$\lambda_1$	$D$	$E(B - V)$	$T_{\text{eff}} \pm \Delta T_{\text{eff}}$	$\theta \pm \Delta\theta$	$\gamma$	$T_{\text{eff}}(\lambda_1, D)$
29248	B2IV	51.2	0.144	0.048	23610±1530	0.262±0.022	1.00	23120
29305	B7V	61.3	0.328	0.021	12120±530	0.603±0.010	1.00	13030
30211	B4IV	45.0	0.248	0.024	15770±890	0.346±0.015	1.00	16510
30614	B0.5Ia	32.0	0.057	0.277	25340±1670	0.274±0.023	0.95	22620
31647	A1V	76.0	0.455	0.032	9750±330	0.346±0.007	1.00	9950
32309	B9V	63.0	0.425	0.018	10800±420	0.315±0.008	1.00	10960
32549	B9IV	45.1	0.438	0.000	9520±320	0.392±0.007	1.00	11040
32630	B4V	59.0	0.232	0.020	17940±1070	0.460±0.017	1.00	17390
33802	B6V	59.5	0.299	0.028	13280±640	0.336±0.011	1.00	14140
33904	B7IV	49.6	0.331	0.015	12390±550	0.590±0.010	1.00	13390
33949	B7III	41.3	0.358	0.033	12750±590	0.358±0.010	1.00	12710
34085	B8Ia	12.0	0.177	0.058	12130±530	2.713±0.010	1.18	12330
34503	B6IV	44.8	0.303	0.045	14450±770	0.470±0.012	1.00	14440
35468	B2III	49.0	0.146	0.023	21840±1390	0.775±0.021	1.00	22530
35497	B5.5IV	44.0	0.288	0.022	13960±710	1.116±0.011	1.00	14910
35600	A0Ib	18.0	0.375	0.288	10870±420	0.324±0.008	0.69	10260
36267	B5V	60.9	0.257	0.020	16020±910	0.314±0.015	1.00	15930
36371	B5Ia	15.0	0.129	0.471	15370±860	0.476±0.014	1.17	14060
36512	O8-9V	68.1	0.079	0.029	32340±2220	0.142±0.025	1.00	32060
36822	B0IV	55.0	0.095	0.111	28340±1900	0.198±0.024	1.00	29330
37128	B0Ib	39.1	0.060	0.059	24670±1620	0.681±0.022	1.16	24440
37468	O9.5V	71.0	0.082	0.061	31270±2130	0.230±0.025	1.00	31420
37481	B2V	61.0	0.142	0.035	24350±1590	0.101±0.022	1.00	24700
37744	B2V	65.0	0.141	0.057	25690±1700	0.088±0.023	1.00	25000
38666	O8-9V	66.5	0.072	0.017	31510±2150	0.111±0.025	1.00	33170
38771	B0II	46.0	0.081	0.057	23170±1500	0.620±0.022	1.00	26730
39970	B9Ib-Ia	12.0	0.261	0.487	11530±480	0.349±0.009	1.51	11250
40111	B1Ib	38.0	0.084	0.183	24660±1620	0.197±0.022	1.22	22950
40183	A1V	69.0	0.485	0.012	8910±280	1.506±0.007	1.00	9680
40312	B9IV	47.0	0.448	0.000	9890±340	0.959±0.008	1.00	10850
40589	B9Ib	12.0	0.284	0.378	11660±490	0.295±0.009	1.33	10970
41117	B2Ia	24.0	0.050	0.494	20740±1310	0.371±0.020	1.53	20640
41753	B4V	55.0	0.229	0.032	18800±1140	0.251±0.018	1.00	17560
42087	B3Ia	25.0	0.102	0.384	16460±940	0.258±0.015	1.18	17440
43112	B1V	58.0	0.117	0.032	27900±1870	0.091±0.024	1.00	27190
43384	B4Ia	20.0	0.125	0.621	14780±800	0.304±0.013	1.38	15140
44743	B1III	45.0	0.112	0.036	25320±1670	0.586±0.023	1.00	23690
46300	A1Ib	17.0	0.421	0.083	9800±340	0.455±0.007	1.00	9740
46769	B7III-II	30.0	0.288	0.151	13930±710	0.210±0.011	0.45	12990
47105	A1.5IV	61.0	0.518	0.001	9040±280	1.435±0.007	1.00	9280
47240	B1Ib	35.0	0.090	0.372	21540±1370	0.157±0.021	1.33	21670
47432	O8-9Ib	43.0	0.050	0.389	25620±1690	0.133±0.023	1.77	28550
47670	B7III	33.0	0.331	0.014	12120±530	0.625±0.010	1.09	12760
47964	B7IV-III	42.0	0.347	0.021	12100±530	0.193±0.009	1.00	13040
48434	B0II	44.0	0.072	0.241	25290±1670	0.128±0.023	1.87	26770
48977	B3V	60.0	0.210	0.039	19590±1210	0.125±0.019	1.00	18820
49567	B4III	37.0	0.209	0.051	17270±1010	0.125±0.016	1.11	17110
52089	B1III	45.0	0.120	0.034	22010±1400	0.801±0.021	1.30	23240
53138	B4Ia	22.0	0.130	0.038	14920±820	0.580±0.013	1.00	15620
53244	B6III	41.9	0.289	0.033	13690±690	0.378±0.011	1.00	14830
58350	B5Ia	19.0	0.152	0.012	12670±580	0.882±0.010	1.00	14180
66811	O6-7III	55.3	0.051	0.043	37250±2630	0.371±0.027	1.00	36630
67797	B4IV	50.9	0.251	0.028	16680±960	0.280±0.016	1.00	16450
68520	B5IV	46.0	0.287	0.022	14090±730	0.326±0.011	1.00	14950

Table 2: continued.

HD	SpT/LC	$\lambda_1$	$D$	$E(B - V)$	$T_{\text{eff}} \pm \Delta T_{\text{eff}}$	$\theta \pm \Delta\theta$	$\gamma$	$T_{\text{eff}}(\lambda_1, D)$
71155	A1V	74.0	0.467	0.025	10060±360	0.538±0.008	1.00	9800
74280	B2IV-V	53.3	0.189	0.019	19410±1200	0.254±0.019	1.00	20080
77327	A1III	47.0	0.509	0.008	9080±290	0.691±0.007	1.00	9790
79447	B3IV	50.5	0.220	0.015	17250±1010	0.333±0.016	1.00	18010
79469	A0V	63.7	0.441	0.023	10980±430	0.490±0.009	1.00	10630
83754	B5V	59.1	0.253	0.024	16150±920	0.211±0.015	1.00	16220
83944	B9V	66.2	0.410	0.006	11550±480	0.335±0.009	1.00	11150
86440	B6II	25.0	0.232	0.049	13980±720	0.493±0.011	1.18	13650
87737	A0Ib	18.0	0.411	0.053	9820±340	0.685±0.007	1.00	9900
89021	A1V	64.0	0.488	0.006	8790±270	0.754±0.007	1.00	9730
91316	B1.5Ib	34.8	0.094	0.056	19830±1230	0.312±0.020	1.21	21370
95418	>A1V	70.0	0.496	0.004	9470±310	1.112±0.007	1.00	9480
97633	>A1V	67.0	0.510	0.022	9180±290	0.772±0.007	1.00	9280
98664	B9IV	54.4	0.438	0.023	10680±410	0.466±0.008	1.00	10970
98718	B5V	60.1	0.261	0.014	16760±970	0.346±0.016	1.00	15730
100600	B3V	58.0	0.218	0.033	18230±1090	0.129±0.018	1.00	18280
100841	A1III	34.6	0.518	0.020	9880±340	0.768±0.008	1.00	9720
100889	B9V	57.2	0.435	0.021	11280±460	0.334±0.009	1.00	10940
106625	B7IV	49.4	0.348	0.009	12360±550	0.799±0.010	1.00	12820
106911	B4V	58.2	0.238	0.026	15330±850	0.321±0.014	1.00	17060
108767	A0.5V	71.0	0.448	0.020	10580±400	0.777±0.008	1.00	10270
109026	B4V	58.9	0.227	0.027	16740±970	0.357±0.016	1.00	17700
111123	B1IV	54.3	0.125	0.041	27030±1800	0.780±0.023	1.00	25740
112185	A1IV	58.0	0.511	0.000	9240±300	1.504±0.007	1.00	9530
112413	B7V	59.0	0.335	0.021	11630±490	0.718±0.009	1.00	12890
116656	A1V	67.0	0.470	0.033	9340±300	1.361±0.007	1.00	9980
120315	B4V	61.0	0.227	0.015	17870±1060	0.832±0.017	1.00	17710
123299	A0IV	53.0	0.482	0.025	10430±390	0.571±0.008	1.00	10190
129056	B2IV	47.8	0.145	0.041	23100±1490	0.537±0.022	1.00	22380
129246	>A1V	79.0	0.488	0.000	8990±280	0.611±0.007	1.00	9220
132058	B2IV	52.1	0.148	0.024	24090±1570	0.436±0.022	1.00	23000
135742	B7.5IV	44.0	0.363	0.022	12300±550	0.801±0.010	1.00	12500
137422	>A2III	35.0	0.562	0.022	8280±240	1.022±0.009	0.48	9110
139006	A1V	69.0	0.476	0.026	9900±340	1.175±0.008	1.00	9820
141003	A1V	69.0	0.479	0.018	8810±270	0.682±0.007	1.00	9770
144217	B1V	65.5	0.115	0.210	30540±2080	0.505±0.024	1.00	27750
145389	B8.5V	65.0	0.363	0.040	11700±490	0.407±0.009	1.00	12030
147394	B5V	53.0	0.262	0.034	16350±940	0.356±0.015	1.00	15900
148112	A0IV	57.0	0.458	0.072	9810±340	0.417±0.007	1.00	10520
149438	B0IV	58.4	0.095	0.040	31440±2150	0.333±0.025	1.00	29640
149881	B0.5III-II	45.0	0.094	0.070	23420±1520	0.063±0.022	1.35	24720
155125	>A1V	75.0	0.478	0.000	8620±260	1.205±0.008	1.00	9570
155763	B6IV	45.0	0.314	0.026	13420±660	0.586±0.011	1.00	14080
158094	B7V	53.4	0.343	0.020	12360±550	0.508±0.010	1.00	12840
159975	B8III	35.5	0.360	0.243	12790±590	0.428±0.010	0.94	12470
160578	B1.5III	50.1	0.131	0.033	24720±1620	0.492±0.022	1.12	23780
160762	B3IV	51.0	0.211	0.036	19100±1170	0.330±0.019	1.00	18590
164353	B5Ib	23.8	0.181	0.185	15420±860	0.045±0.014	1.11	14790
166182	B2.5III	43.0	0.174	0.074	22420±1440	0.232±0.021	1.00	19870
169022	A0III	45.5	0.498	0.024	9520±320	1.468±0.007	1.00	9960
172167	A1V	66.0	0.489	0.000	9470±310	3.292±0.007	1.00	9670
173300	B7IV	44.8	0.332	0.118	14990±830	0.597±0.014	1.00	13490
175191	B2.5V	62.1	0.187	0.000	18890±1150	0.711±0.018	1.00	20370
176437	A1III	32.0	0.493	0.040	10000±350	0.740±0.008	1.00	10000

Table 2: continued.

HD	SpT/LC	$\lambda_1$	$D$	$E(B - V)$	$T_{\text{eff}} \pm \Delta T_{\text{eff}}$	$\theta \pm \Delta\theta$	$\gamma$	$T_{\text{eff}}(\lambda_1, D)$
177724	A1V	66.0	0.493	0.052	9830±340	0.865±0.007	1.00	9600
177756	B9V	58.9	0.396	0.004	11780±500	0.558±0.009	1.00	11600
179761	B8V-IV	52.4	0.364	0.073	13060±620	0.268±0.010	1.00	12320
182255	B5V	56.0	0.268	0.030	15300±850	0.208±0.014	1.00	15520
186882	A0IV	50.0	0.479	0.031	10150±360	0.858±0.008	1.00	10280
188209	B0Ib	42.0	0.065	0.159	25260±1670	0.124±0.023	1.33	26040
191692	B9IV	52.0	0.462	0.011	10340±380	0.712±0.008	1.00	10570
192425	A1V	77.0	0.461	0.033	9120±290	0.370±0.007	1.00	9810
192907	A0V	59.0	0.451	0.023	10500±390	0.408±0.008	1.00	10570
195556	B4II	33.0	0.204	0.128	17680±1040	0.236±0.017	1.07	16320
195810	B6IV	48.0	0.303	0.032	14540±780	0.370±0.012	1.00	14370
196867	B9IV	53.0	0.417	0.018	11220±450	0.512±0.009	1.00	11370
197345	A2Ia	4.0	0.366	0.056	8720±260	2.255±0.008	1.70	8630
198001	>A1V-IV	64.0	0.529	0.021	9370±310	0.612±0.007	1.00	8980
198478	B4Ia	20.0	0.109	0.562	15390±860	0.517±0.014	1.21	15880
199081	B4V-IV	51.0	0.248	0.028	16180±920	0.240±0.015	1.00	16590
202850	B9.5Ia	10.0	0.265	0.200	11170±450	0.536±0.009	1.78	11110
204172	B0II-Ib	42.0	0.073	0.142	24110±1570	0.110±0.022	1.36	25370
205021	B1V	59.0	0.120	0.037	26920±1790	0.312±0.023	1.00	26960
206672	B3III	43.0	0.208	0.089	18360±1100	0.241±0.018	1.27	18150
207260	A2Ia	6.0	0.378	0.506	8980±280	1.010±0.007	1.00	8790
207330	B3III	44.0	0.190	0.078	17890±1060	0.301±0.017	1.00	19270
207971	B7IV	47.1	0.338	0.011	12520±570	0.649±0.010	1.00	13230
209481	O6-7IV	57.0	0.062	0.348	30570±2080	0.149±0.024	1.00	34280
209744	B1III	50.0	0.120	0.363	25440±1680	0.112±0.023	1.00	24510
209819	B8V	64.3	0.348	0.020	12310±550	0.376±0.010	1.00	12320
209952	B5V	51.7	0.282	0.013	13920±710	1.084±0.011	1.00	14990
209961	B2IV	49.0	0.180	0.159	21100±1330	0.119±0.020	1.00	20420
209975	B1Ia	32.0	0.063	0.331	24720±1620	0.222±0.022	0.45	22190
210191	B4III	38.8	0.202	0.040	17890±1060	0.140±0.017	1.08	17750
210418	>A1V	76.0	0.480	0.033	8840±270	0.747±0.007	1.00	9500
212061	A0V	64.5	0.458	0.022	10490±390	0.527±0.008	1.00	10280
212120	B5V	55.0	0.282	0.050	15250±850	0.288±0.014	1.00	14900
212593	B8.5II	21.0	0.299	0.179	11150±440	0.441±0.009	1.53	11370
212883	B2.5IV-III	48.0	0.183	0.085	20400±1280	0.101±0.020	1.00	20140
212978	B2III	46.0	0.176	0.081	20990±1320	0.113±0.020	1.00	20360
213420	B2III	44.0	0.167	0.131	19750±1230	0.267±0.019	1.00	20460
213558	A1.5V	75.0	0.465	0.038	9840±340	0.590±0.007	1.00	9800
213976	B2V	64.0	0.165	0.105	22800±1470	0.073±0.021	1.00	22170
213998	B9V	58.5	0.397	0.017	11740±500	0.434±0.009	1.00	11590
214240	B5III	43.0	0.265	0.126	16330±930	0.139±0.015	1.00	15750
214652	B2V	60.0	0.183	0.105	22350±1430	0.081±0.021	1.00	20730
214680	O6-7V	65.0	0.068	0.089	32380±2220	0.136±0.025	1.00	33820
214923	B9IV	50.3	0.420	0.005	11430±470	0.581±0.009	1.00	11360
214993	B1III	49.0	0.120	0.111	24130±1570	0.155±0.022	1.00	24260
214994	A0.5V	62.0	0.477	0.050	9930±350	0.364±0.008	1.00	9970
215191	B2IV	52.0	0.145	0.131	22800±1470	0.099±0.021	1.00	23230
217101	B2V	63.0	0.151	0.093	22760±1460	0.107±0.021	1.00	23700
217811	B4III	45.0	0.225	0.217	19330±1190	0.132±0.019	1.00	17420
218045	A1IV	55.0	0.500	0.021	9850±340	1.036±0.008	1.00	9850
218376	B0.5III	46.0	0.095	0.244	27100±1810	0.204±0.023	1.28	25190
218407	B3V	60.0	0.184	0.174	21200±1340	0.101±0.020	1.00	20650
219688	B5V	51.8	0.266	0.021	15260±850	0.297±0.014	1.00	15730
222173	B8IV	44.0	0.371	0.038	12620±580	0.369±0.010	1.00	12340

Table 2: continued.

HD	SpT/LC	$\lambda_1$	$D$	$E(B - V)$	$T_{\text{eff}} \pm \Delta T_{\text{eff}}$	$\theta \pm \Delta\theta$	$\gamma$	$T_{\text{eff}}(\lambda_1, D)$
222661	B9.5V	66.0	0.428	0.021	10860±420	0.381±0.008	1.00	10820
223640	B6.5V	55.9	0.321	0.000	11740±500	0.260±0.009	1.00	13510
224990	B5V	54.2	0.259	0.032	16100±910	0.215±0.015	1.00	16030

The parameter  $\lambda_1$  is given as  $\lambda_1 - 3700 \text{ \AA}$ .

The notation >SpT/LC means that the spectral type is cooler than the indicated one.

Table 5: Compilation of effective temperatures determined for the program stars by other authors.

HD	$T_{\text{eff}}^f$	$T_{\text{eff}}^{(1)}$	$T_{\text{eff}}^{(2)}$	$T_{\text{eff}}^{(3)}$	$T_{\text{eff}}^{(4)}$	$T_{\text{eff}}^{(5)}$	$T_{\text{eff}}^{(6)}$
358	12750	–	–	–	–	–	–
886	21870	–	21990	–	–	21250	–
2905	22160	–	–	21600	–	24000	22500
3360	21850	–	22210	–	–	–	–
3369	15980	15520	–	–	–	–	–
4142	16430	16670	–	–	–	–	–
4727	16290	15850	–	–	–	–	–
11241	22080	25350	–	–	–	–	–
12767	13250	–	–	–	–	–	–
12953	9750	–	–	–	–	–	–
13267	14380	–	–	–	–	15000	–
14055	9440	–	–	–	9490	–	–
14228	12470	12900	–	–	13080	–	–
14489	9840	–	–	–	–	–	–
14818	18300	–	–	–	–	20000	18250
15130	9920	–	–	–	9890	–	–
15318	10630	–	–	–	10600	–	–
16046	10910	–	–	–	–	–	–
16582	23160	–	23570	–	–	–	–
16908	17520	16850	–	–	16940	–	–
17081	13680	13210	13040	–	13170	13100	–
17573	12980	12570	–	–	12400	–	–
18604	13940	13240	–	–	–	–	–
19356	12800	14290	–	–	–	–	–
20041	10800	–	–	–	–	–	–
21291	11420	–	–	–	–	11500	–
21364	13040	12650	–	–	12540	–	–
21389	11040	–	–	–	–	–	–
21447	9240	–	–	–	–	–	–
21790	11760	–	–	–	–	–	–
21856	25370	25880	–	–	–	–	–
22928	14890	–	13940	–	14200	–	–
22951	29330	28970	–	–	–	–	–
23180	22840	22860	–	–	–	–	–
23227	16230	–	–	–	–	–	–
23288	14020	–	–	–	–	–	–
23324	13220	12760	–	–	–	–	–
23338	14180	–	–	–	–	–	–
23408	14310	–	–	–	–	–	–
23625	23980	25530	–	–	–	–	–
23753	12680	–	–	–	–	–	–
23850	13020	–	–	–	–	–	–
23923	11640	–	–	–	–	–	–
24131	29130	28380	–	–	–	–	–
24398	22040	–	19870	19900	–	23000	–
24431	27370	–	–	–	–	–	–
24760	27160	25760	–	–	–	–	–
25204	16970	–	–	–	–	–	–
25490	8990	–	–	–	9260	9250	–
27376	12460	–	–	–	–	–	–
27396	16720	–	16800	–	–	–	–
27962	8680	–	–	–	–	9000	–

Table 5: continued.

HD	$T_{\text{eff}}^f$	$T_{\text{eff}}^{(1)}$	$T_{\text{eff}}^{(2)}$	$T_{\text{eff}}^{(3)}$	$T_{\text{eff}}^{(4)}$	$T_{\text{eff}}^{(5)}$	$T_{\text{eff}}^{(6)}$
29248	23610	–	23500	21600	–	–	–
29305	12120	–	–	–	–	–	–
30211	15770	15540	14950	–	15630	–	–
30614	25400	–	25000	26300	–	32500	29000
31647	9750	–	–	–	–	–	–
32309	10800	–	10200	–	–	–	–
32549	9520	–	10200	–	–	–	–
32630	17940	17020	17580	–	17050	16380	–
33802	13280	–	11860	–	–	–	–
33904	12390	–	–	–	–	–	–
33949	12750	11690	–	–	–	–	–
34085	12130	–	11660	–	–	13000	–
34503	14450	13510	14260	–	14620	–	–
35468	21840	21040	21760	20900	21940	–	–
35497	13960	13650	13820	–	13490	–	–
35600	10870	–	–	–	–	11000	–
36267	16020	17100	–	–	–	–	–
36371	15370	–	–	–	–	16500	–
36512	32340	–	34350	–	–	–	–
36822	28340	–	–	–	31120	–	–
37128	24670	–	24960	26400	–	28500	27250
37468	31270	–	31560	–	–	–	–
37481	24350	24550	–	–	–	–	–
37744	25690	24830	–	–	–	–	–
38666	31510	–	–	–	–	–	–
38771	23170	–	26390	23100	–	27500	26250
39970	11530	–	–	–	–	–	–
40111	24660	–	–	21400	–	–	–
40183	8910	–	–	–	–	–	–
40312	9890	–	–	–	–	–	–
40589	11660	–	–	–	–	–	–
41117	20740	–	17460	–	–	19500	19000
41753	18800	16970	17410	–	17640	–	–
42087	16460	–	–	–	–	20500	18000
43112	27900	28510	–	–	–	–	–
43384	14780	–	–	–	–	–	–
44743	25320	–	25500	24700	–	–	–
46300	9800	–	–	–	–	–	–
46769	13930	14520	–	–	–	–	–
47105	9040	–	9260	–	9380	9150	–
47240	21540	20610	–	–	–	–	–
47432	25620	–	–	–	–	–	–
47670	12120	11910	11610	–	11950	–	–
47964	12100	–	–	–	–	–	–
48434	25290	24270	–	–	–	–	–
48977	19590	19770	–	–	–	–	–
49567	17270	17100	–	–	–	–	–
52089	22010	–	21830	21000	–	–	–
53138	14920	–	14760	–	–	18500	16000
53244	13690	–	13600	–	–	–	–
58350	12670	–	13150	–	–	16000	15000
66811	37250	–	33760	35100	–	–	–
67797	16680	–	15460	–	–	–	–

Table 5: continued.

HD	$T_{\text{eff}}^f$	$T_{\text{eff}}^{(1)}$	$T_{\text{eff}}^{(2)}$	$T_{\text{eff}}^{(3)}$	$T_{\text{eff}}^{(4)}$	$T_{\text{eff}}^{(5)}$	$T_{\text{eff}}^{(6)}$
68520	14090	14420	–	–	–	–	–
71155	10060	–	–	–	–	–	–
74280	19410	18680	18790	–	18650	–	–
77327	9080	–	–	–	–	–	–
79447	17250	17220	–	–	–	–	–
79469	10980	–	–	–	10640	–	–
83754	16140	–	15400	–	–	–	–
83944	11550	10740	–	–	–	–	–
86440	13980	13300	–	–	–	–	–
87737	9820	–	–	–	–	–	–
89021	8790	–	–	–	9160	9000	–
91316	19830	–	–	20300	–	–	22000
95418	9470	–	9170	–	9650	9600	–
97633	9180	–	–	–	9130	9250	–
98664	10680	–	–	–	–	–	–
98718	16760	–	–	–	–	–	–
100600	18230	19320	–	–	–	–	–
100841	9880	–	10470	–	–	–	–
100889	11280	–	–	–	10810	–	–
106625	12360	–	12450	–	–	–	–
106911	15330	–	–	–	–	–	–
108767	10580	–	–	–	–	–	–
109026	16740	–	15510	–	–	–	–
111123	27030	–	27600	–	–	–	–
112185	9240	–	–	–	–	–	–
112413	11630	–	–	–	–	–	–
116656	9340	–	–	–	–	–	–
120315	17870	17360	16770	–	17100	16900	–
123299	10430	–	–	–	–	10000	–
129056	23100	20320	–	–	–	–	–
129246	8990	–	–	–	–	–	–
132058	24090	–	23780	22800	–	–	–
135742	12300	12060	–	–	12310	12130	–
137422	8280	–	–	–	–	–	–
139006	9900	–	–	–	–	–	–
141003	8810	–	–	–	–	–	–
144217	30540	–	–	–	–	–	–
145389	11700	–	10860	–	–	–	–
147394	16350	15030	15210	–	15050	15000	–
148112	9810	–	–	–	–	–	–
149438	31440	–	–	31800	29920	–	–
149881	23420	21130	–	–	29280	–	–
155125	8620	–	–	–	–	–	–
155763	13420	–	12960	–	13090	–	–
158094	12360	11480	12010	–	–	–	–
159975	12790	–	11650	–	–	–	–
160578	24720	–	25780	24400	–	–	–
160762	19100	17640	17810	–	17460	–	–
164353	15420	13490	–	–	–	16500	15500
166182	22420	21380	20320	–	–	–	–
169022	9520	–	9460	–	9540	–	–
172167	9470	–	9660	–	9620	–	–
173300	14990	12390	–	–	12110	–	–

Table 5: continued.

HD	$T_{\text{eff}}^f$	$T_{\text{eff}}^{(1)}$	$T_{\text{eff}}^{(2)}$	$T_{\text{eff}}^{(3)}$	$T_{\text{eff}}^{(4)}$	$T_{\text{eff}}^{(5)}$	$T_{\text{eff}}^{(6)}$
175191	18890	–	18990	–	–	–	–
176437	10000	–	–	–	9830	9550	–
177724	9830	–	9480	–	9550	9500	–
177756	11780	11560	11410	–	11430	–	–
179761	13060	–	–	–	–	13000	–
182255	15300	–	–	–	–	–	–
186882	10150	–	9880	–	10180	–	–
188209	25260	–	31080	27700	–	–	–
191692	10340	–	–	–	10170	–	–
192425	9120	–	–	–	–	–	–
192907	10500	–	10650	–	–	10250	–
195556	17680	–	18140	–	–	–	–
195810	14540	13550	13610	–	–	–	–
196867	11220	–	10820	–	10910	–	–
197345	8720	–	–	–	–	–	–
198001	9370	–	–	–	9180	9200	–
198478	15390	–	14270	–	–	18000	17170
199081	16180	16560	–	–	–	–	–
202850	11170	–	–	–	–	–	11000
204172	24110	–	–	25200	–	28500	28500
205021	26920	–	25780	26200	–	–	–
206672	18360	17390	17890	–	17110	–	–
207260	8980	–	–	–	–	–	–
207330	17890	17100	–	–	–	–	–
207971	12520	12170	11800	–	11950	–	–
209481	30570	–	–	–	–	–	–
209744	25440	–	–	–	–	–	–
209819	12310	12470	11280	–	–	–	–
209952	13920	13450	13660	–	13930	–	–
209961	21100	21430	–	–	–	–	–
209975	24720	–	–	–	–	32500	–
210191	17890	–	–	–	–	–	–
210418	8840	–	–	–	–	–	–
212061	10490	–	–	–	10290	–	–
212120	15250	14580	–	–	14690	–	–
212593	11150	–	9930	–	–	–	11800
212883	20400	22700	–	–	–	–	–
212978	20990	20370	–	–	20790	–	–
213420	19750	19850	20840	–	20490	–	–
213558	9840	–	–	–	9600	–	–
213976	22800	–	–	–	–	–	–
213998	11740	11490	11220	–	11530	–	–
214240	16330	17380	–	–	–	–	–
214652	22350	21930	–	–	–	–	–
214680	32380	–	33560	–	33110	33000	–
214923	11430	11320	–	–	11500	–	–
214993	24130	23600	–	–	–	–	–
214994	9930	–	–	–	9560	9530	–
215191	22800	22930	–	–	24050	–	–
217101	22760	23120	–	–	–	–	–
217811	19330	19100	–	–	–	–	–
218045	9850	–	–	–	9850	–	–
218376	27100	–	27470	–	–	29000	–

Table 5: continued.

HD	$T_{\text{eff}}^f$	$T_{\text{eff}}^{(1)}$	$T_{\text{eff}}^{(2)}$	$T_{\text{eff}}^{(3)}$	$T_{\text{eff}}^{(4)}$	$T_{\text{eff}}^{(5)}$	$T_{\text{eff}}^{(6)}$
218407	21200	23230	–	–	–	–	–
219688	15260	–	15210	–	14910	–	–
222173	12610	11850	11870	–	11870	–	–
222661	10860	–	–	–	–	–	–
223640	11740	–	–	–	–	–	–
224990	16100	–	–	–	15330	–	–

$T_{\text{eff}}^{(1)}$  : Gulati et al. (1989),Castelli (1991)  
 $T_{\text{eff}}^{(2)}$  : Underhill et al. (1979), Code et al. (1976), Malagnini et al. (1986)  
 $T_{\text{eff}}^{(3)}$  : Remie & Lamers (1981)  
 $T_{\text{eff}}^{(4)}$  : Morossi & Malagnini (1985), Malagnini et al. (1983), Malagnini & Morossi (1990)  
 $T_{\text{eff}}^{(5)}$  : McErlean et al. (1999), Adelman et al. (2002)  
 $T_{\text{eff}}^{(6)}$  : Searle et al. (2008), Markova & Puls (2008), Crowther et al. (2006)

### List of Objects

- ‘HD 41117’ on page 4
- ‘HD 41117’ on page 6
- ‘HD 172167’ on page 8
- ‘HD 130109’ on page 8
- ‘HD 120315’ on page 8
- ‘HD 30614’ on page 12
- ‘HD 37128’ on page 12
- ‘HD 38771’ on page 12